iScience

CellPress
OPEN ACCESS

Article

# Fatty Acid Synthesis Is Indispensable for Survival of Human Pluripotent Stem Cells

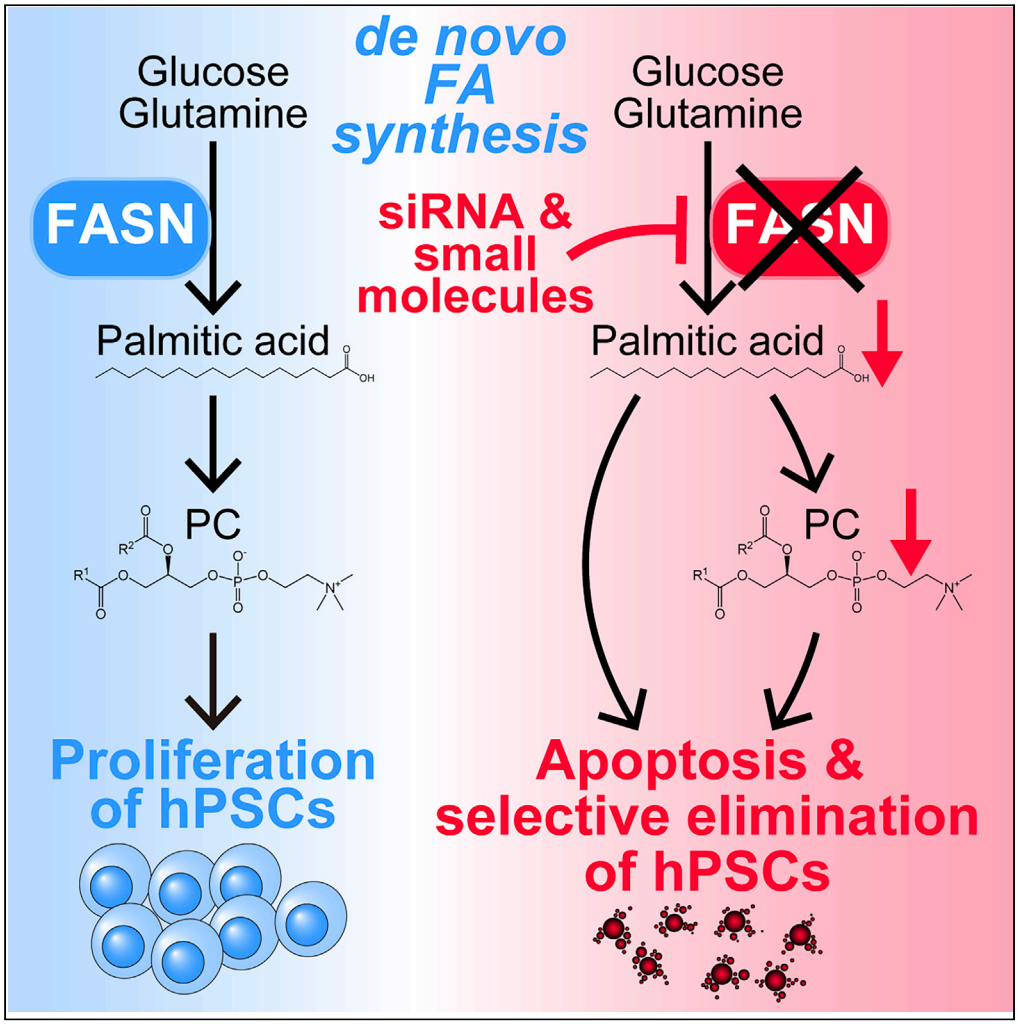


Sho Tanosaki, Shugo Tohyama, Jun Fujita, ..., Minoru S.H. Ko, Makoto Suematsu, Keiichi Fukuda

shugotohyama@keio.jp (S.T.)
jfujita@keio.jp (J.F.)

## HIGHLIGHTS

Undifferentiated hPSCs upregulate *de novo* FA synthesis-related enzymes

Inhibition of *de novo* FA synthesis induces cell death in undifferentiated hPSCs

Phosphatidylcholine is the key metabolite required for hPSC survival

FASN inhibition eliminates undifferentiated hPSCs from hPSC derivatives

Tanosaki et al., iScience *23*, 101535
September 25, 2020 
https://doi.org/10.1016/j.isci.2020.101535

iScience

CellPress
OPEN ACCESS

Article

# Fatty Acid Synthesis Is Indispensable for Survival of Human Pluripotent Stem Cells

Sho Tanosaki,[1,2] Shugo Tohyama,[1,3,11,*] Jun Fujita,[1,4,*] Shota Someya,[1,2] Takako Hishiki,[5,6] Tomomi Matsuura,[6] Hiroki Nakanishi,[8] Takayo Ohto-Nakanishi,[8] Tomohiko Akiyama,[7] Yuika Morita,[1] Yoshikazu Kishino,[1] Marina Okada,[1] Hidenori Tani,[1] Yusuke Soma,[1] Kazuaki Nakajima,[1] Hideaki Kanazawa,[1] Masahiro Sugimoto,[9,10] Minoru S.H. Ko,[7] Makoto Suematsu,[5] and Keiichi Fukuda[1]

## SUMMARY

**The role of lipid metabolism in human pluripotent stem cells (hPSCs) is poorly understood. We have used large-scale targeted proteomics to demonstrate that undifferentiated hPSCs express different fatty acid (FA) biosynthesis-related enzymes, including ATP citrate lyase and FA synthase (FASN), than those expressed in hPSC-derived cardiomyocytes (hPSC-CMs). Detailed lipid profiling revealed that inhibition of FASN resulted in significant reduction of sphingolipids and phosphatidylcholine (PC); moreover, we found that PC was the key metabolite for cell survival in hPSCs. Inhibition of FASN induced cell death in undifferentiated hPSCs via mitochondria-mediated apoptosis; however, it did not affect cell survival in hPSC-CMs, neurons, or hepatocytes as there was no significant reduction of PC. Furthermore, we did not observe tumor formation following transplantation of FASN inhibitor-treated cells. Our findings demonstrate the importance of *de novo* FA synthesis in the survival of undifferentiated hPSCs and suggest applications for FASN inhibition in regenerative medicine.**

## INTRODUCTION

Human pluripotent stem cells (hPSCs), including human embryonic stem cells (hESCs) and human induced pluripotent stem cells (hiPSCs), are capable of self-renewing, proliferating, and differentiating into cells of the three germ layers (Takahashi et al., 2007; Thomson et al., 1998). Regenerative therapy using hPSCs holds promise for many diseases resistant to conventional medical therapies, including progressive heart failure, retinal diseases, and central nervous system diseases (Mandai et al., 2017; Nakamura and Okano, 2013; Yoshida and Yamanaka, 2017). However, to provide safe and effective regenerative therapy, it is essential to obtain highly qualified target cells from hPSCs.

As metabolism plays a key role in the pluripotency, self-renewal, and survival of hPSCs, metabolic regulation enables several efficient and cost-effective techniques, including generation of hiPSCs, differentiation into required cell types, and elimination of residual undifferentiated stem cells (Ben-David et al., 2013; Cornacchia et al., 2019; Shiraki et al., 2014; Sone et al., 2017; Tohyama et al., 2013, 2016; Yanes et al., 2010). Similar to cancer cells, hPSCs show activated glycolysis even under sufficiently aerobic conditions, a phenomenon referred to as the Warburg effect. However, recent studies have raised questions on this classical dogma in cancer cells, in that specific amino acids and fatty acids (FAs) are essential for maintenance of cancer stemness and progression. In hPSCs, the importance of amino acids (e.g., glutamine, methionine, and kynurenine) has also been reported (Shiraki et al., 2014; Tohyama et al., 2016; Yamamoto et al., 2019). In contrast to glucose and amino acid metabolism, little is known about the role of lipid metabolism in hPSCs.

We screened expression profiles of metabolic enzymes in hiPSCs and hiPSC-derived differentiated cardiomyocytes (hiPSC-CMs) by large-scale targeted proteomics, the results from which demonstrated that FA synthase (FASN) is expressed at the highest levels in hiPSCs but not in hiPSC-CMs. FASN is the final enzyme in the *de novo* FA synthesis pathway and is upregulated in cancer cells that originate in multiple tissues, including mammary glands, prostate, and lungs (Ali et al., 2018; De Schrijver et al., 2003; Pizer et al., 2000).

[1]Department of Cardiology, Keio University School of Medicine, Shinjuku, Tokyo 160-8582, Japan

[2]Department of Emergency and Critical Care Medicine, Keio University School of Medicine, Shinjuku, Tokyo 160-8582, Japan

[3]Department of Organ Fabrication, Keio University School of Medicine, Shinjuku, Tokyo 160-8582, Japan

[4]Endowed Course for Severe Heart Failure Treatment II, Keio University School of Medicine, Shinjuku, Tokyo 160-8582, Japan

[5]Department of Biochemistry, Keio University School of Medicine, Shinjuku, Tokyo 160-8582, Japan

[6]Clinical and Translational Research Center, Keio University School of Medicine, Shinjuku, Tokyo 160-8582, Japan

[7]Department of Systems Medicine, Keio University School of Medicine, Shinjuku, Tokyo 160-8582, Japan

[8]Lipidome Lab Co., Ltd., Akita 010-0825, Japan

[9]Research and Development Center for Minimally Invasive Therapies Health Promotion and Preemptive Medicine, Tokyo Medical University, Shinjuku, Tokyo 160-8402, Japan

[10]Institute for Advanced Biosciences, Keio University, Tsuruoka, Yamagata 997-0052, Japan

[11]Lead Contact

*Correspondence: shugotohyama@keio.jp (S.T.), jfujita@keio.jp (J.F.)

https://doi.org/10.1016/j.isci.2020.101535

Lipids play a wide variety of roles in cell physiology, as energy sources, signaling molecules, protein modification, and cellular components, although these roles vary between cell types. Specifically in hESCs, a mixture of lipids stimulates their self-renewal (Garcia-Gonzalo and Izpisua Belmonte, 2008). Also, it has been reported that FA synthesis activation is critical for the maintenance of pluripotency by promoting mitochondrial fission (Wang et al., 2017). Meanwhile, during the reprogramming of embryonic fibroblasts into induced pluripotent stem cells, the gene expression profiles as well as the metabolic profiles become dramatically altered (Folmes et al., 2011; Meissen et al., 2012; Wu et al., 2019). In regard to lipids, the cytidine diphosphate-ethanolamine pathway contributes to reprogramming mouse embryonic fibroblasts into mouse induced pluripotent stem cells (Wu et al., 2019). A recent report also showed that *de novo* FA synthesis skewed hPSCs toward a naive-to-primed intermediate state by inhibiting endogenous ERK (Cornacchia et al., 2019). Despite the importance of FA synthesis, detailed lipid profiles and their roles in hPSC survival remain unknown. Therefore, in this study, we determined metabolic features, lipid profiles, and the role of FA synthesis in hPSCs relative to their derivatives. We then applied our findings to the improvement of regenerative medicine.

## RESULTS

### FASN Is Upregulated in Undifferentiated hPSCs

To identify unique metabolic features of hPSCs, we performed large-scale targeted proteomics with a focus on metabolism-related enzymes in hiPSCs and hiPSC-CMs as representative differentiated cells. The proteomic data revealed distinct differences between the two cell types (Figures 1A and 1B). The differentially expressed proteins included ATP citrate lyase (ACLY) and FASN, both involved in *de novo* FA synthesis (Figures 1B and 1C). Moreover, undifferentiated hiPSCs showed higher levels of enzymes involved in the pentose phosphate and serine synthesis pathways (Figures S1A and S1B); meanwhile, hiPSC-CMs had higher concentrations of enzymes involved in the tricarboxylic acid (TCA) cycle, FA oxidation, and oxidative phosphorylation (Figures 1C and S1C–S1E).

These differences suggest that hiPSC-CMs are highly catabolic, whereas undifferentiated hiPSCs are highly anabolic, likely reflecting the differences between non-proliferating and proliferating states, respectively. We also confirmed the difference in FASN expression by immunocytochemistry and western blotting (Figures 1D–1F). These data suggest that undifferentiated hiPSCs express higher amounts of enzymes in anabolic pathways, particularly those involved in *de novo* FA synthesis, compared with hiPSC-CMs. Therefore, we focused on FASN, which generates palmitic acid (Pal) from acetyl-CoA, malonyl-CoA, and NADPH, and sought to investigate its significance in hPSCs.

### Pal Is Required for the Survival of Undifferentiated hPSCs

To investigate the role of FASN in hPSC proliferation and survival, *FASN* expression was knocked down using small interfering RNA (siRNA) (Figures 2A and 2B). The knockdown significantly inhibited hiPSC proliferation, whereas supplementation with Pal, the product of FASN, restored proliferation (Figures 2C and 2D).

In addition to knockdown by siRNA, we also utilized a pharmacological approach to inhibit FASN. Orlistat, an anti-obesity drug approved by the US Food and Drug Administration in the United States and other countries, inhibits FASN and suppresses the proliferation of cancer cells expressing high levels of FASN (Kridel et al., 2004). Expectedly, orlistat induced cell death in hESCs and hiPSCs (Figure 2E). This effect was greatly attenuated by Pal supplementation, suggesting that the cytotoxic effect was mediated by a decrease in Pal, and not by any off-target effect (Figures 2F and 2G). Furthermore, two FASN inhibitors, FASN-IN-2 and FT-113, were found to induce cell death in hiPSCs (Figure S2A). Similarly, an ACLY inhibitor, SB204990, induced cell death of undifferentiated hiPSCs (Figure S2B). However, although the effect of the FASN inhibitors were attenuated by supplementation of external Pal, that of the ACLY inhibitor was not. This difference likely arose from the wide range of applications assigned to acetyl-CoA, as it is used not only for *de novo* FA synthesis but also for other reactions, including acetylation of various proteins (e.g., histones) (Wellen et al., 2009).

Next, to determine the mechanism of cell death induced by orlistat, we performed time-lapse imaging of orlistat-treated cells and observed activation of caspase 3/7 within 12 h of initiation of treatment, suggesting apoptosis (Figure 2H). As FASN links glycolysis, TCA cycle, and glutaminolysis with lipid metabolism, its inhibition would theoretically cause dramatic alterations in these processes (Figure 2I). Hence, to

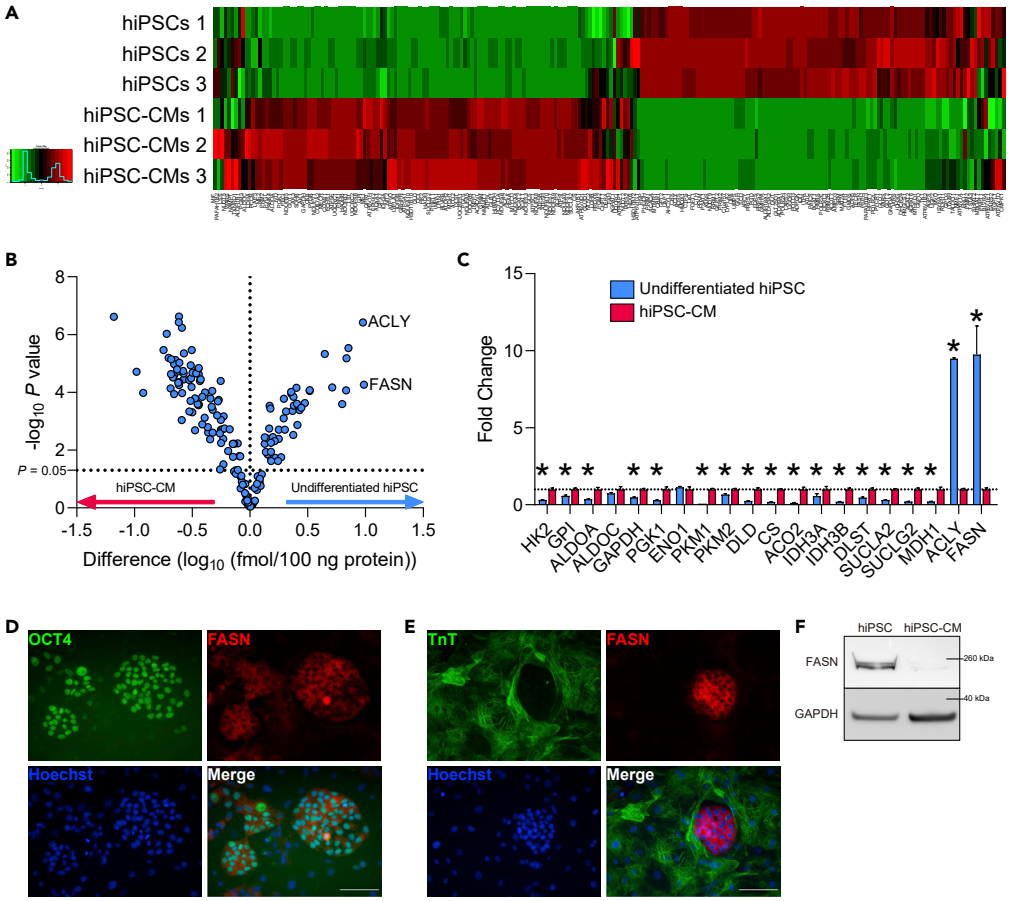


**Figure 1. FASN Is Highly Expressed in Undifferentiated hPSCs**

(A) Heatmap of proteomic analysis of undifferentiated hiPSCs (253G4) and hiPSC (253G4)-CMs (n = 3).

(B) Volcano plot of proteomic analysis of undifferentiated hiPSCs (253G4) and hiPSC (253G4)-CMs. Protein levels were transformed to log10 scale. Student's t test was performed for each protein (n = 3).

(C) Relative abundance of enzymes involved in glycolysis, TCA cycle, and *de novo* FA synthesis compared with hiPSC (253G4)-CMs in proteomic analysis. Student's t test was performed for each protein (n = 3).

(D and E) (D) and (E) Representative image of immunocytochemistry of cocultured hiPSCs (253G4) and hiPSC (253G4)-CMs. Scale bars, 100 μm.

(F) Representative image of western blot of hiPSCs (253G4) and hiPSC (253G4)-CMs.

Data are presented as means ± SD; *p < 0.05.

determine the effects of pharmacological FASN inhibition on metabolism, we performed capillary electrophoresis and mass spectrometry (CE-MS)-based metabolomics. Inhibition of FASN by orlistat resulted in significant accumulation of citrate and malonyl-CoA, which is one of the upstream metabolites in *de novo* FA synthesis, confirming successful inhibition of FASN (Figure 2J). However, the increase observed for citrate was dramatically higher than that for malonyl-CoA. Hence, to exclude the possibility of alteration in activities of ACLY and ACC under orlistat treatment, we performed western blotting, which did not show significant change in phosphorylation of ACLY or ACC, suggesting activation and inhibition, respectively (Figure S2C). Citrate can be synthesized from glucose and glutamine. Glutamine-derived citrate is synthesized via two pathways: oxidative TCA cycle (forward) and reductive carboxylation via cytosolic isocitrate dehydrogenase 1 (IDH1) (reverse), which produces citrate from glutamine by consuming NADPH (Figure 2K). To evaluate the pathway from which the observed increase in citrate was derived, we performed metabolic flux analysis with either [U-$^{13}$C]-glucose ($^{13}C_6$ Glc) or [U-$^{13}$C]-glutamine ($^{13}C_5$ Gln) in orlistat-untreated or orlistat-treated hiPSCs (Figure 2K). A dramatic increase was observed in citrate derived from both glucose and glutamine (Figures 2L, 2M, and S2D). Focusing on the citrate derived from $^{13}C_6$ Glc, a large proportion of the labeled form was determined to be m+2, which is derived from glycolytic

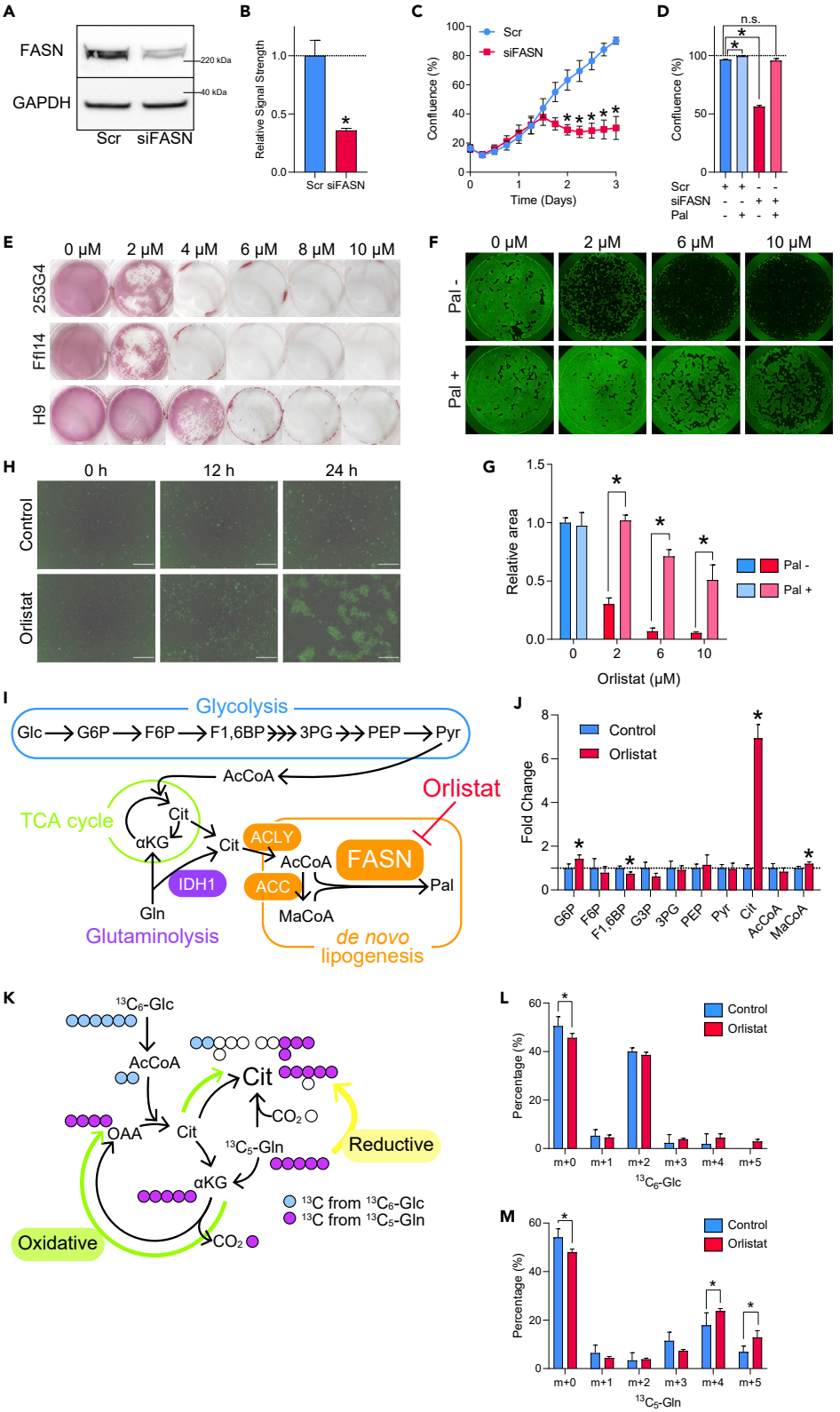
A
FASN
GAPDH
220 kDa
40 kDa
Scr siFASN
B
Relative Signal Strength
Scr siFASN
C
Scr
siFASN
Confluence (%)
Time (Days)
D
n.s.
Confluence (%)
Scr
siFASN
Pal
E
0 μM 2 μM 4 μM 6 μM 8 μM 10 μM
253G4
Ff14
H9
F
0 μM 2 μM 6 μM 10 μM
Pal -
Pal +
H
0 h 12 h 24 h
Control
Orlistat
G
Relative area
Pal -
Pal +
Orlistat (μM)
I
Glycolysis
Glc G6P F6P F1,6BP 3PG PEP Pyr
AcCoA
Orlistat
TCA cycle
Cit
αKG
Cit
ACLY
AcCoA
FASN
IDH1
ACC
Pal
Gln
MaCoA
Glutaminolysis
de novo
lipogenesis
J
Control
Orlistat
Fold Change
G6P F6P F1,6BP G3P 3PG PEP Pyr Cit AcCoA MaCoA
K
13C6-Glc
AcCoA
Cit
CO2
OAA
Cit
13C5-Gln
Reductive
αKG
13C from 13C6-Glc
13C from 13C5-Gln
Oxidative
CO2
L
Control
Orlistat
Percentage (%)
m+0 m+1 m+2 m+3 m+4 m+5
13C6-Glc
M
Control
Orlistat
Percentage (%)
m+0 m+1 m+2 m+3 m+4 m+5
13C5-Gln

**Figure 2. Palmitic Acid Is Essential for the Survival of Undifferentiated hPSCs**

(A) Representative western blot image for FASN and GAPDH of hiPSCs (253G4) after treatment with Scr or *FASN* siRNAs.

(B) Quantification of relative FASN content compared with GAPDH by western blot. Student's t test, n = 3.

(C) Growth of hiPSCs (253G4) treated with Scr RNA or *FASN* siRNAs. Holm-Sidak test was performed for each time point (n = 3).

(D) Confluence at 72 h after introduction of either Scr RNA or *FASN* siRNA to hiPSCs (253G4) with or without 50 μM Pal 24 h after introduction of RNAs. The same concentration of BSA (8.3 μM) was used as control. One-way ANOVA with Dunnett's test was performed with Scr RNA without Pal as control (n = 3).

(E) Alkaline phosphatase (AP) staining of hESCs (H9) and hiPSCs (253G4 and Ff14) treated with orlistat of the indicated concentrations for 72 h.

(F) Representative images of hiPSCs (253G4) cultured in 12-well plates stained with calcein AM after treatment with orlistat at the indicated concentrations for 24 h with or without 50 μM Pal. The same concentration of BSA (8.3 μM) was used as control for Pal.

(G) Quantification of hiPSC (253G4) relative cell area after treatment with orlistat at the indicated concentrations for 24 h, with or without 50 μM Pal. The same concentration of BSA (8.3 μM) was used as a control for Pal. Student's t test was performed to compare the presence and absence of Pal at each concentration of orlistat (n = 3).

(H) Detection of apoptosis by IncuCyte Caspase-3/7 Green Reagent staining following orlistat treatment. Scale bar, 200 μm.

(I) Metabolic pathway from glucose to Pal via glycolysis, glutaminolysis, TCA cycle, and *de novo* lipogenesis.

(J) CE-MS of intermediate metabolites in *de novo* FA synthesis from glucose after 3 h of 6 μM orlistat treatment. Data are normalized to controls. Student's t test was performed for each metabolite (n = 3). G6P, glucose 6-phosphate; F6P, fructose 6-phosphate, F1,6BP, fructose 1,6-bisphosphate; G3P, glyceraldehyde 3-phosphate; PEP, phosphoenolpyruvate; Pyr, pyruvate; Gln, glutamine, αKG, α-ketoglutarate; AcCoA, acetyl-CoA; MaCoA, malonyl-CoA; ACLY, ATP citrate lyase; ACC, acetyl-CoA carboxylase; IDH1, isocitrate dehydrogenase 1.

(K) Metabolic pathway from glucose and glutamine to citrate via glycolysis, TCA cycle, and glutaminolysis. The major labeled form of citrate produced from $^{13}C_6$-glucose, $^{13}C_5$-glutamine via oxidative pathway, and glutamine via reductive pathway are m+2, m+4, and m+5, respectively.

(L) Percentage of labeled citrate formed after 1 h of orlistat treatment with $^{13}C_6$-glucose. Student's t test was performed for each labeled form of citrate (n = 3).

(M) Percentage of labeled citrate formed after 1 h of orlistat treatment with $13C_5$-glutamine. Student's t test was performed for each labeled form of citrate (n = 3).

Data are presented as means ± SD; *p < 0.05.

acetyl-CoA and oxaloacetate (Figures 2L and S2D). Meanwhile, the labeled form of citrate derived from $^{13}C_5$ Gln was m+4 citrate, which is derived from glutamine via the forward TCA cycle and glycolytic acetyl-CoA (Figures 2M and S2D). Cumulatively, these data indicate that the major contributor to the observed citrate increase was glucose-derived acetyl-CoA and forward TCA cycle-derived oxaloacetate, which are converted to citrate in the mitochondrial matrix. Therefore, although we cannot distinguish the localization of citrate in our CE-MS-based metabolome analysis, considering that citrate must be transported from the mitochondrial matrix to the cytosol for *de novo* FA synthesis, the dramatic increase in citrate may suggest accumulation of citrate in the mitochondrial matrix. Hence, as the biosynthesis of acetyl-CoA and malonyl-CoA takes place in the cytosol, we postulated that this is the mechanism responsible for the observed discrepancy in the increase in citrate and malonyl-CoA.

In the metabolic flux analysis using $^{13}C_5$ Gln, we found that the percentage of m+5 citrate was significantly increased, suggesting that the reductive pathway was also activated (Figures 2M and S2D). Citrate generated from glutamine via reductive carboxylation can be utilized for *de novo* FA synthesis depending on the cell type and culture conditions (Jiang et al., 2016; Metallo et al., 2011; Yoo et al., 2008). The increase in the reductive pathway may suggest a possible role for IDH1-mediated citrate biosynthesis as an $NADP^+$ recycling mechanism to compensate for the reduced NADPH consumption caused by FASN inhibition. Meanwhile, in rapidly growing cancer cells with defective mitochondria, this reductive pathway contributes to *de novo* FA synthesis (Mullen et al., 2011). Therefore, activation of the reductive pathway may suggest that FASN inhibition causes mitochondrial dysfunction.

Next, considering that citrate reportedly inhibits tumor growth (Newsholme et al., 1985; Ren et al., 2017), to exclude the possibility of citrate-induced growth inhibition and cell death, we supplemented external citrate and quantified the intracellular citrate level. We then confirmed that the increase in intracellular citrate was not associated with cell proliferation or survival in hPSCs (Figures S2E and S2F). We also quantified the intracellular citrate level when Pal was supplemented with orlistat and confirmed that the citrate level

remained elevated despite Pal supplementation (Figure S2G). These data suggest that accumulation of citrate is not the mechanism responsible for inducing cell death following FASN inhibition.

Regarding the relationship between metabolism, epigenetics, and pluripotency in hPSCs, Moussaieff et al. reported that glucose-derived cytosolic acetyl-CoA supports the maintenance of pluripotent status through histone acetylation, whereas decreased acetyl-CoA levels induce differentiation (Moussaieff et al., 2015). To evaluate the acetylation status of orlistat-treated hPSCs, we examined the acetylation of histone H3 lysine 27 by western blotting and confirmed that it was not significantly changed (Figure S2H). In addition, no significant change was observed in the expression of pluripotent markers OCT4, NANOG, and TRA1-60, as assessed by immunocytochemistry and flow cytometry (Figures S2I and S2J). Cumulatively, these results indicate that orlistat does not affect the pluripotent status of hPSCs.

Previous studies suggested that inhibition of carnitine palmitoyl transferase 1, via accumulation of malonyl-CoA, is the mechanism by which orlistat induces cell death (Thupari et al., 2001). To determine whether hiPSCs utilize FA oxidation, we supplemented the hPSC maintenance medium with albumin-bound [U-$^{13}$C]-labeled palmitic acid ($^{13}C_{16}$-Pal) for 72 h and quantified $^{13}C_{16}$-Pal-derived metabolites by CE-MS. We did not detect significant levels of $^{13}$C in TCA cycle metabolites irrespective of orlistat treatment, indicating that hiPSCs did not utilize FA oxidation (**data not shown**), consistent with a previous report (Zhang et al., 2016). These data suggest that Pal is an indispensable metabolite for the proliferation and survival of hiPSCs, in a manner that is independent of its utilization as a fuel source.

## Inhibition of FASN Leads to Decreased Phosphatidylcholine

As Pal is utilized in a broad range of lipid metabolism, we performed liquid chromatography-MS-based lipidomics to evaluate changes in downstream metabolites caused by FASN inhibition (Figures 3A and 3B). Previous studies reported that the accumulation of ceramides (Cers), which are regarded as proapoptotic lipids in some cell lines, following FASN inhibition contributes to cell death, because inhibition of FASN could be rescued by coadministration of the Cer synthase inhibitor fumonisin B1 (FB1) or the serine palmitoyltransferase inhibitor myriocin (Alwarawrah et al., 2016; Bandyopadhyay et al., 2006; Obeid et al., 1993; Pizer et al., 2000; Thupari et al., 2001). Surprisingly, we did not observe accumulation of Cers, rather we observed significant reduction in their levels (Figure 3B). Ceramide-1-phosphate (Cer1P), formed from Cer by ceramide kinase, is associated with survival and proliferation and was found to be concomitantly decreased (Figure 3B). To ascertain the significance of the decrease in these two sphingolipids (SLs), we supplemented the medium with them. However, SL supplementation did not attenuate the effect of orlistat (Figure S3A). In addition, inhibition of *de novo* Cer synthesis by FB1 alone did not induce cell death in hiPSCs (Figure S3B). Thus, we concluded that the decrease in Cer or Cer1P does not mediate cell death caused by FASN inhibition.

Among glycerophospholipids, we observed a significant decrease in phosphatidylcholine (PC) and lysophosphatidylcholine (Figure 3B). In contrast, the levels of phosphatidylethanolamine, phosphatidylinositol, and phosphatidylserine were not significantly changed (Figure S3C). PC is a major component of lipid bilayers, including cellular membranes; its production via *de novo* FA synthesis increases during cytokinesis (Scaglia et al., 2014). It is worth noting that 3 h of FASN inhibition caused a significant decrease in PC, because cells contain abundant PC. To determine the physiological significance of this distinct decrease in PC among glycerophospholipids, we supplemented PC with orlistat and confirmed that exogenous PC attenuated the effect of FASN inhibition (Figures 3C and 3D), suggesting that the decrease in PC plays a key role in cell death induced by FASN inhibition. Moreover, PC with relatively short fatty acyl chains were decreased by orlistat treatment, presumably reflecting a decreased flow of FAs synthesized *de novo* to PC metabolism. Concordant with this hypothesis, unlike the lipid profiles of hiPSCs, PC was not significantly changed in hiPSC-CMs following 3 h of orlistat treatment, suggesting that its reduction in undifferentiated hPSCs is due to its dependency on *de novo* FA synthesis for proliferation (Figure S3D). This finding is consistent with the previous study described earlier that demonstrated the importance of PC production via *de novo* FA synthesis in cytokinesis (Scaglia et al., 2014).

## FASN Inhibition Induces Cytochrome *c* Release and Caspase-3 Activation

The initiation of apoptosis is primarily regulated by intrinsic and extrinsic pathways. To identify the pathway critical in the cell death induced following FASN inhibition, we measured the levels of cytochrome *c* and observed significant increases in cytoplasmic fractions (Figures 3E, 3F, and S3E). Next, moving upstream

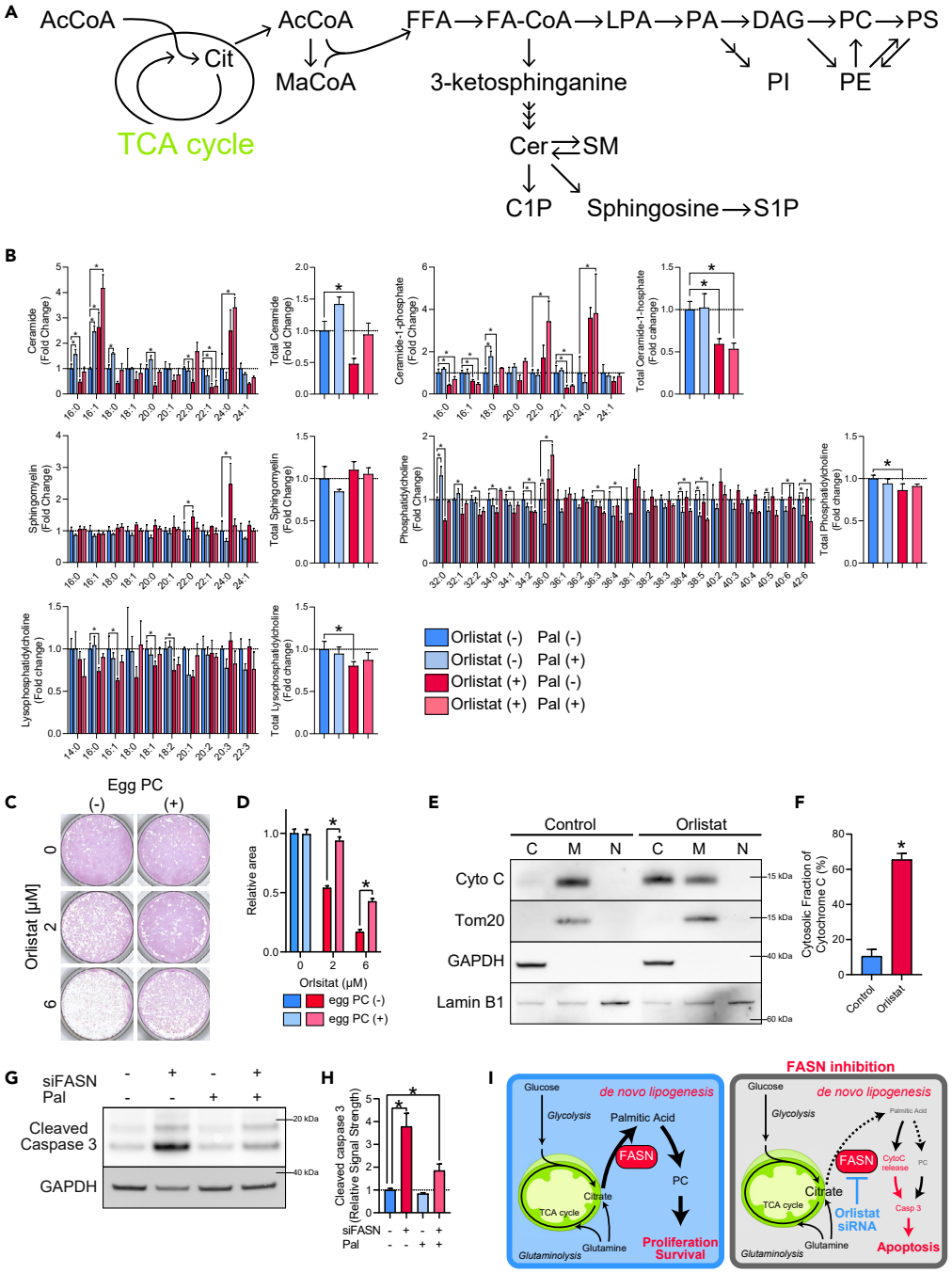


**Figure 3. Metabolomic Analysis under FASN Inhibition and Mechanism of Cell Death**

(A) Metabolic pathway from TCA cycle to various lipids. FFA, free fatty acid; FA-CoA, fatty acyl-CoA; LPA, lysophosphatidic acid; PA, phosphatidic acid; DAG, diacylglycerol; PC, phosphatidylcholine; PS, phosphatidylserine; PI, phosphatidylinositol; PS, phosphatidylserine; SM, sphingomyelin; S1P, sphingosine-1-phosphate.

(B) Liquid chromatography-MS of glycerolipids and SLs after 3 h of 6 μM orlistat treatment with or without 50 μM Pal. Data are normalized to controls without orlistat or Pal. Numbers indicate carbon chain lengths followed by degrees of desaturation. One-way ANOVA with Dunnett's test was performed with orlistat (–) Pal (–) as control (n = 3).

(C) Representative image of AP staining of hiPSCs (253G4) after 24 h of orlistat and chicken egg PC treatment.

(D) Quantification of relative AP-positive cell area in hiPSCs (253G4) after 24 h of orlistat and chicken egg PC treatment. Student's t test was performed for each concentration of orlistat (n = 3).

**Figure 3. *Continued***

(E) Representative western blot image of cytochrome *c* subcellular localization in hiPSCs (253G4) 12 h after orlistat treatment. Cyto C, cytochrome *c*.

(F) Cytosolic fraction of cytochrome *c* of hiPSCs (253G4) 12 h after orlistat treatment quantified by western blotting. Student's t test, n = 3.

(G) Representative western blotting image of hiPSCs (253G4) 48 h after transfection with either Scr RNA or *FASN* siRNA. Pal (50 μM) was supplemented 24 h after transfection.

(H) Relative amount of cleaved caspase 3 in hiPSCs (253G4) 48 h after transfection with either Scr RNA or *FASN* siRNA quantified by western blotting. Pal (50 μM) was supplemented 24 h after transfection. Signal strengths were standardized using those of GAPDH. One-way ANOVA with Dunnett's test was performed with Scr RNA and without Pal as a control (n = 3).

(I) Schematic of metabolic features of undifferentiated hPSCs and consequences of FASN inhibition.

Data are presented as means ± SD; *p < 0.05.

from cytochrome *c*, we measured levels of Noxa and Bid. We found that Noxa was increased, whereas Bid was not changed by orlistat treatment (Figures S3F and S3G). Expectedly, *FASN* knockdown increased cleaved caspase-3 levels in hPSCs, which were greatly attenuated by both Pal and PC supplementation (Figures 3G, 3H, and S3H). These data indicate that the mitochondrial intrinsic pathway plays a primary role in FASN inhibition-induced apoptosis. This is consistent with our CE-MS analysis and a previous study that reported that during mitochondrial dysfunction, reductive carboxylation of glutamine supports *de novo* FA synthesis, as described previously (Figure 2M) (Mullen et al., 2011). Among the upstream components involved in the intrinsic pathway activation, we did not observe any activation of the endoplasmic reticulum (ER) stress response or accumulation of p53 (Figures S3I and S3J). Taken together, our findings indicate that whereas undifferentiated hPSCs upregulate *de novo* lipid synthesis for proliferation, FASN inhibition results in caspase 3-mediated apoptosis via cytochrome *c* release and decrease in PC level (Figure 3I).

### Orlistat Induces Cell Death in Undifferentiated hiPSCs, but Not in hiPSC Derivatives

To determine whether orlistat treatment affects cell survival in hPSC derivatives, including cardiomyocytes, hepatocytes, and neurons, we cultured these cells with orlistat for 72 h. We found that orlistat did not affect cell survival in any of the three differentiated cell types (Figures 4A and S4). Next, to determine whether orlistat treatment could eliminate hPSCs in mixtures with other cell types, we cocultured undifferentiated hiPSCs with hiPSC-CMs with or without orlistat. In contrast to controls, which produced substantial numbers of OCT4-positive colonies, orlistat killed OCT4-positive cells, whereas hiPSC-CMs survived (Figures 4B and 4C). In addition, we administered orlistat to a mixed cell population, composed of neuronal fate-decided cells as well as residual undifferentiated hiPSCs, during neuronal differentiation using synthetic mRNAs. As a result, we succeeded in eliminating OCT4-positive cells and purifying hiPSC-derived neurons (Figures 4D and 4E). These results suggest a possibility for using orlistat to eliminate undifferentiated hPSCs in multiple cellular lineages.

Last, we tested whether pretreatment with orlistat prevented tumor formation in immunocompromised, non-obese diabetic-severe combined immunodeficient (NOD-SCID) mice. Undifferentiated hiPSCs were cocultured with human dermal fibroblasts at a ratio of 2:100 with or without orlistat for 72 h and then subcutaneously transplanted into NOD-SCID mice. Pretreatment with orlistat prevented teratoma formation 8 weeks after transplantation (Figures 4F–4H).

## DISCUSSION

In this study, we demonstrated that undifferentiated hPSCs express high levels of *de novo* FA synthesis enzymes relative to hiPSC-CMs. Inhibition of *de novo* FA synthesis induced apoptotic death of undifferentiated hPSCs via a significant reduction in PC. *De novo* FA synthesis sustains proliferation by providing building material, whereas it is noteworthy that its inhibition induced cell death, not only cell-cycle arrest, in undifferentiated hPSCs.

Metabolic signatures of hPSCs are known to be similar to those of cancer cells (Zhang et al., 2012). Consistent with this dogma, *de novo* FA synthesis is activated not only in hPSCs but also in some cancer types, including breast, renal, lung, and prostate (Menendez and Lupu, 2007). Therefore, FA synthesis has been regarded as a drug target for these cancers. In cancer cells, several mechanisms of cell death induced by inhibition of FA synthesis have been proposed, including p53-regulated metabolic stress,

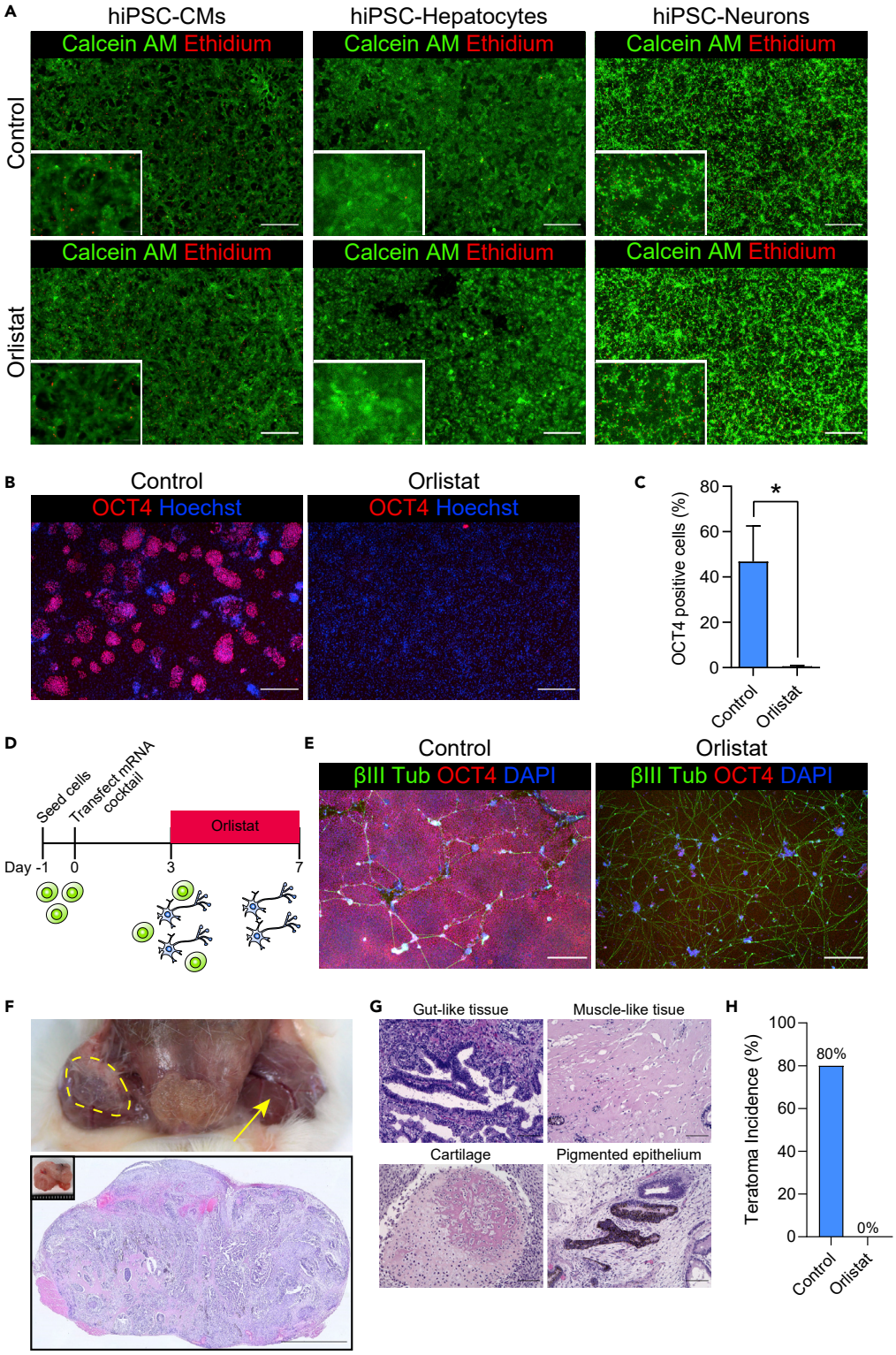


**Figure 4. Orlistat Eliminates Undifferentiated Pluripotent Stem Cells and Prevents Teratoma Formation**

(A) Viability of differentiated cells under 6 μM orlistat for 72 h. Live and dead cells were identified using calcein AM and ethidium, respectively. Scale bars, 500 μm and 100 μm.

**Figure 4. *Continued***

(B) Selective elimination by orlistat of OCT4-positive undifferentiated hiPSCs (253G4) cocultured with hiPSC (253G4)-CMs. Scale bar, 500 μm.

(C) Quantification of OCT4-positive cells. Student's t test, n = 3.

(D) Schematic of neural differentiation using synthetic mRNAs.

(E) Representative images of hiPSC (201B7)-derived neurons treated with or without orlistat for 96 h. Scale bar, 500 μm.

(F–H) Assay of orlistat treatment using a mouse teratoma model. (F) Macroscopic (top) and microscopic (bottom) overviews of teratomas. Dotted line and yellow arrow indicate tumor formation by control (cells without orlistat treatment) and no tumor formation by orlistat treatment, respectively. Scale bar, 2 mm. (G) Representative images of teratoma histology. Scale bar, 100 μm. (H) Orlistat treatment prevents teratoma incidence (n = 5).

Data are presented as means ± SD; *$p < 0.05$.

Cer accumulation, inhibition of anti-apoptotic proteins, and disturbance of membrane function, but detailed mechanisms remain poorly understood (Menendez and Lupu, 2007). In this study, we demonstrated that the apoptosis induced by inhibition of FASN in hPSCs was not mediated by p53-regulated metabolic stress or Cer accumulation. Sterol regulatory element-binding transcription factor 1 (SREBF1) regulates lipid metabolism including *de novo* FA synthesis in some cancer cells (Wu and Naar, 2019). However, although SREBF1 is upregulated during somatic cell reprogramming, introduction of *Srebf1* did not activate *de novo* FA synthesis-related genes in mouse induced pluripotent stem cells (Wu et al., 2016). Instead, SREBF1 activated the expression of pluripotent genes by interacting with MYC (Wu et al., 2016). Hence, inhibition of SREBF1 in hPSCs may influence the pluripotent state of the cells instead of cytotoxicity.

Notably, detailed lipid profiling revealed that not only PC but also Cer and Cer1P were significantly decreased by orlistat treatment. Although previous studies reported accumulation of Cer as the mechanism of cell death upon FASN inhibition, the observed decrease in Cer reported in the present study was reasonable because *de novo* Cer synthesis requires palmitoyl-CoA as one of the substrates, which is presumably decreased by the inhibition of FASN. We also found that PC supplementation increased the survival of orlistat-treated hPSCs, but SL supplementation did not, suggesting that PC is a key metabolite for survival of hPSCs. As PC is an important factor in the maintenance of membrane function, decreases in PC induced cytochrome *c* release from mitochondria, leading to apoptotic hPSC death. It is worth noting that that there was a trend that PC with relatively short fatty acyl chains were sensitive to orlistat treatment compared with PC with longer fatty acyl chains. PC with different acyl chains has distinct properties and affects membrane properties including curvature, charge, fluidity, and local architecture (Bi et al., 2019). In fact, PC is dynamically remodeled by lysophosphatidylcholine acyltransferases (LPCAT). In intestinal stem cells, loss of LPCAT3 decreases the abundance of PC with saturated fatty acyl chains, which ultimately results in increased cell proliferation (Wang et al., 2018). Alternatively, gain of LPCAT1 increases saturated PC, leading to cell proliferation via activated epidermal growth factor receptor signaling in non-small cell lung cancer (Bi et al., 2019). Meanwhile, our lipidomics revealed a difference in the degree of susceptibility to FASN inhibition in PC depending on the fatty acyl chains. Although the consequence of altered LPCAT activity seems to be context dependent as described earlier, FASN inhibition may alter membrane properties, and hence signaling pathway activities, that affect cellular viability.

Here, we developed a method to selectively eliminate hPSCs from hPSC derivatives based on differences in lipid metabolism. Although many methods have been reported to reduce hPSC contamination of hPSC derivatives to realize safer regenerative medicine, a metabolic approach has several advantages in terms of scalability, simplicity, and cost. We previously developed a method to eliminate residual undifferentiated hPSC contamination of hPSC-CMs that exploited differences in glucose, lactate, and glutamine metabolism (Tohyama et al., 2013, 2016). However, this method cannot be applied to hepatocytes, neurons, and several other cell types because they cannot survive when depleted of glucose and glutamine even under existence of lactate. In contrast, inhibiting FA synthesis did not affect the viability of differentiated cardiomyocytes, neurons, and hepatocytes, suggesting that this approach can be applied elsewhere. It has been reported that inhibition of stearoyl-CoA desaturase kills hPSCs via ER stress (Ben-David et al., 2013; Li et al., 2017). Theoretically, inhibition of FASN, which acts upstream of stearoyl-CoA desaturase, may also induce cell death by the same pathway. However, we did not observe an activation of the ER stress response (Figure S3I), indicating that inhibition of FASN acts differently than inhibition of stearoyl-CoA desaturase.

Many clinical trials using hPSCs are underway. However, the risk of tumorigenicity is still one of the major barriers to the clinical application of regenerative medicine. To date, glucose and amino acid metabolism of hPSCs and their derivatives have been analyzed in detail and exploited to efficiently eliminate hPSCs from hPSC derivatives (Shiraki et al., 2014; Tohyama et al., 2013, 2016). A deeper understanding of the metabolic differences in lipid metabolism between hPSCs and their derivatives will contribute significantly to the realization of safer regenerative medicine.

### Limitations of the Study

Although the activation of reductive carboxylation pathway of glutamine upon FASN inhibition suggests mitochondrial dysfunction, the mechanism linking FASN inhibition and mitochondrial dysfunction remains unclear. Further work unveiling this missing link definitely will advance our knowledge about the role of lipid metabolism in mitochondrial homeostasis. In addition, although we have demonstrated that FASN inhibition can be rescued by supplementation of PC, its effect was modest compared with that of Pal. Hence, we cannot exclude other underlying mechanisms leading to cell death following FASN inhibition. Further studies will be required to uncover the role of *de novo* synthesized FAs in the wide variety of lipids.

### Resource Availability

#### *Lead Contact*

Further information and requests for resources and reagents should be directed to and will be fulfilled by the Lead Contact, Shugo Tohyama, Keio University (shugotohyama@keio.jp).

#### *Materials Availability*

This study did not generate new unique reagents.

#### *Data and Code Availability*

There is no dataset and/or code associated with the article.

## METHODS

All methods can be found in the accompanying Transparent Methods supplemental file.

## SUPPLEMENTAL INFORMATION

Supplemental Information can be found online at https://doi.org/10.1016/j.isci.2020.101535.

## ACKNOWLEDGMENTS

The authors thank the Center for iPSC Research and Application, and Kyoto University, for providing hiPSC lines (253G4, 201B7, and Ff14). The authors thank Hideo Shindou and Takao Shimizu for their assistance in liposome preparation. The present work was mainly supported by Projects for Technological Development, Research Center Network for Realization of Regenerative Medicine by Japan, the Japan Agency for Medical Research and Development (AMED) grant 19bm0404023h0002 to S.T., and partly supported by the Highway Program for Realization of Regenerative Medicine from AMED grant 19bk0104062h0003 to K.F. and JSPS KAKENHI grant 17H05067 to S.T. Infrastructure of metabolomics based on CE-MS was supported by Japan Science and Technology ERATO Suematsu Gas Biology (M.S. was the lead from 2010 to 2015).

## AUTHOR CONTRIBUTIONS

S. Tohyama conceptualized and designed the study; S. Tanosaki performed and analyzed most experiments; S.S., H.N., T.O.-N., T.H., T.A., K.N., Y.K., M.O., Y.M., H.T., Y.S., and H.K. contributed to specific experiments; S. Tanosaki and S. Tohyama wrote the original draft; S. Tohyama, J.F., and K.F. wrote, reviewed, and edited the manuscript; S. Tohyama, J.F., and K.F. acquired funding; S. Tohyama, J.F., M.S.H.K., M.S., and K.F. supervised the study.

## DECLARATION OF INTERESTS

S. Tanosaki, S. Tohyama, J.F., and K.F. have a patent pending related to this work. K.F. is a co-founder and CEO of Heartseed, Inc. S. Tohyama is an advisor of Heartseed, Inc. S. Tohyama, J.F., H.K., and K.F. own equity in Heartseed, Inc. The remaining authors have no conflicts of interest to disclose.

Received: March 6, 2020
Revised: July 26, 2020
Accepted: September 2, 2020
Published: September 25, 2020

## REFERENCES

Ali, A., Levantini, E., Teo, J.T., Goggi, J., Clohessy, J.G., Wu, C.S., Chen, L., Yang, H., Krishnan, I., Kocher, O., et al. (2018). Fatty acid synthase mediates EGFR palmitoylation in EGFR mutated non-small cell lung cancer. EMBO Mol. Med. *10*, e8313.

Alwarawrah, Y., Hughes, P., Loiselle, D., Carlson, D.A., Darr, D.B., Jordan, J.L., Xiong, J., Hunter, L.M., Dubois, L.G., Thompson, J.W., et al. (2016). Fasnall, a selective FASN inhibitor, shows potent anti-tumor activity in the MMTV-Neu model of HER2(+) breast cancer. Cell Chem. Biol. *23*, 678–688.

Bandyopadhyay, S., Zhan, R., Wang, Y., Pai, S.K., Hirota, S., Hosobe, S., Takano, Y., Saito, K., Furuta, E., Iiizumi, M., et al. (2006). Mechanism of apoptosis induced by the inhibition of fatty acid synthase in breast cancer cells. Cancer Res. *66*, 5934–5940.

Ben-David, U., Gan, Q.F., Golan-Lev, T., Arora, P., Yanuka, O., Oren, Y.S., Leikin-Frenkel, A., Graf, M., Garippa, R., Boehringer, M., et al. (2013). Selective elimination of human pluripotent stem cells by an oleate synthesis inhibitor discovered in a high-throughput screen. Cell Stem Cell *12*, 167–179.

Bi, J., Ichu, T.A., Zanca, C., Yang, H., Zhang, W., Gu, Y., Chowdhry, S., Reed, A., Ikegami, S., Turner, K.M., et al. (2019). Oncogene amplification in growth factor signaling pathways renders cancers dependent on membrane lipid remodeling. Cell Metab. *30*, 525–538.

Cornacchia, D., Zhang, C., Zimmer, B., Chung, S.Y., Fan, Y., Soliman, M.A., Tchieu, J., Chambers, S.M., Shah, H., Paull, D., et al. (2019). Lipid deprivation induces a stable, naive-to-primed intermediate state of pluripotency in human PSCs. Cell Stem Cell *25*, 120–136.

De Schrijver, E., Brusselmans, K., Heyns, W., Verhoeven, G., and Swinnen, J.V. (2003). RNA interference-mediated silencing of the fatty acid synthase gene attenuates growth and induces morphological changes and apoptosis of LNCaP prostate cancer cells. Cancer Res. *63*, 3799–3804.

Folmes, C.D., Nelson, T.J., Martinez-Fernandez, A., Arrell, D.K., Lindor, J.Z., Dzeja, P.P., Ikeda, Y., Perez-Terzic, C., and Terzic, A. (2011). Somatic oxidative bioenergetics transitions into pluripotency-dependent glycolysis to facilitate nuclear reprogramming. Cell Metab. *14*, 264–271.

Garcia-Gonzalo, F.R., and Izpisua Belmonte, J.C. (2008). Albumin-associated lipids regulate human embryonic stem cell self-renewal. PLoS One *3*, e1384.

Jiang, L., Shestov, A.A., Swain, P., Yang, C., Parker, S.J., Wang, Q.A., Terada, L.S., Adams, N.D., McCabe, M.T., Pietrak, B., et al. (2016). Reductive carboxylation supports redox homeostasis during anchorage-independent growth. Nature *532*, 255–258.

Kridel, S.J., Axelrod, F., Rozenkrantz, N., and Smith, J.W. (2004). Orlistat is a novel inhibitor of fatty acid synthase with antitumor activity. Cancer Res. *64*, 2070–2075.

Li, J., Condello, S., Thomes-Pepin, J., Ma, X., Xia, Y., Hurley, T.D., Matei, D., and Cheng, J.X. (2017). Lipid desaturation is a metabolic marker and therapeutic target of ovarian cancer stem cells. Cell Stem Cell *20*, 303–314.

Mandai, M., Watanabe, A., Kurimoto, Y., Hirami, Y., Morinaga, C., Daimon, T., Fujihara, M., Akimaru, H., Sakai, N., Shibata, Y., et al. (2017). Autologous induced stem-cell-derived retinal cells for macular degeneration. N. Engl. J. Med. *376*, 1038–1046.

Meissen, J.K., Yuen, B.T., Kind, T., Riggs, J.W., Barupal, D.K., Knoepfler, P.S., and Fiehn, O. (2012). Induced pluripotent stem cells show metabolomic differences to embryonic stem cells in polyunsaturated phosphatidylcholines and primary metabolism. PLoS One *7*, e46770.

Menendez, J.A., and Lupu, R. (2007). Fatty acid synthase and the lipogenic phenotype in cancer pathogenesis. Nat. Rev. Cancer *7*, 763–777.

Metallo, C.M., Gameiro, P.A., Bell, E.L., Mattaini, K.R., Yang, J., Hiller, K., Jewell, C.M., Johnson, Z.R., Irvine, D.J., Guarente, L., et al. (2011). Reductive glutamine metabolism by IDH1 mediates lipogenesis under hypoxia. Nature *481*, 380–384.

Moussaieff, A., Rouleau, M., Kitsberg, D., Cohen, M., Levy, G., Barasch, D., Nemirovski, A., Shen-Orr, S., Laevsky, I., Amit, M., et al. (2015). Glycolysis-mediated changes in acetyl-CoA and histone acetylation control the early differentiation of embryonic stem cells. Cell Metab. *21*, 392–402.

Mullen, A.R., Wheaton, W.W., Jin, E.S., Chen, P.H., Sullivan, L.B., Cheng, T., Yang, Y., Linehan, W.M., Chandel, N.S., and DeBerardinis, R.J. (2011). Reductive carboxylation supports growth in tumour cells with defective mitochondria. Nature *481*, 385–388.

Nakamura, M., and Okano, H. (2013). Cell transplantation therapies for spinal cord injury focusing on induced pluripotent stem cells. Cell Res. *23*, 70–80.

Newsholme, E.A., Crabtree, B., and Ardawi, M.S. (1985). The role of high rates of glycolysis and glutamine utilization in rapidly dividing cells. Biosci. Rep. *5*, 393–400.

Obeid, L.M., Linardic, C.M., Karolak, L.A., and Hannun, Y.A. (1993). Programmed cell death induced by ceramide. Science *259*, 1769–1771.

Pizer, E.S., Thupari, J., Han, W.F., Pinn, M.L., Chrest, F.J., Frehywot, G.L., Townsend, C.A., and Kuhajda, F.P. (2000). Malonyl-coenzyme-A is a potential mediator of cytotoxicity induced by fatty-acid synthase inhibition in human breast cancer cells and xenografts. Cancer Res. *60*, 213–218.

Ren, J.G., Seth, P., Ye, H., Guo, K., Hanai, J.I., Husain, Z., and Sukhatme, V.P. (2017). Citrate suppresses tumor growth in multiple models through inhibition of glycolysis, the tricarboxylic acid cycle and the IGF-1R pathway. Sci. Rep. *7*, 4537.

Scaglia, N., Tyekucheva, S., Zadra, G., Photopoulos, C., and Loda, M. (2014). De novo fatty acid synthesis at the mitotic exit is required to complete cellular division. Cell Cycle *13*, 859–868.

Shiraki, N., Shiraki, Y., Tsuyama, T., Obata, F., Miura, M., Nagae, G., Aburatani, H., Kume, K., Endo, F., and Kume, S. (2014). Methionine metabolism regulates maintenance and differentiation of human pluripotent stem cells. Cell Metab. *19*, 780–794.

Sone, M., Morone, N., Nakamura, T., Tanaka, A., Okita, K., Woltjen, K., Nakagawa, M., Heuser, J.E., Yamada, Y., Yamanaka, S., et al. (2017). Hybrid cellular metabolism coordinated by Zic3 and Esrrb synergistically enhances induction of naive pluripotency. Cell Metab. *25*, 1103–1117.

Takahashi, K., Tanabe, K., Ohnuki, M., Narita, M., Ichisaka, T., Tomoda, K., and Yamanaka, S. (2007). Induction of pluripotent stem cells from adult human fibroblasts by defined factors. Cell *131*, 861–872.

Thomson, J.A., Itskovitz-Eldor, J., Shapiro, S.S., Waknitz, M.A., Swiergiel, J.J., Marshall, V.S., and Jones, J.M. (1998). Embryonic stem cell lines derived from human blastocysts. Science *282*, 1145–1147.

Thupari, J.N., Pinn, M.L., and Kuhajda, F.P. (2001). Fatty acid synthase inhibition in human breast cancer cells leads to malonyl-CoA-induced inhibition of fatty acid oxidation and cytotoxicity. Biochem. Biophys. Res. Commun. *285*, 217–223.

Tohyama, S., Fujita, J., Hishiki, T., Matsuura, T., Hattori, F., Ohno, R., Kanazawa, H., Seki, T., Nakajima, K., Kishino, Y., et al. (2016). Glutamine oxidation is indispensable for survival of human pluripotent stem cells. Cell Metab. *23*, 663–674.

Tohyama, S., Hattori, F., Sano, M., Hishiki, T., Nagahata, Y., Matsuura, T., Hashimoto, H., Suzuki, T., Yamashita, H., Satoh, Y., et al. (2013). Distinct metabolic flow enables large-scale purification of mouse and human pluripotent stem cell-derived cardiomyocytes. Cell Stem Cell *12*, 127–137.

Wang, B., Rong, X., Palladino, E.N.D., Wang, J., Fogelman, A.M., Martin, M.G., Alrefai, W.A., Ford, D.A., and Tontonoz, P. (2018). Phospholipid remodeling and cholesterol availability regulate intestinal stemness and tumorigenesis. Cell Stem Cell *22*, 206–220.

Wang, L., Zhang, T., Wang, L., Cai, Y., Zhong, X., He, X., Hu, L., Tian, S., Wu, M., Hui, L., et al. (2017). Fatty acid synthesis is critical for stem cell pluripotency via promoting mitochondrial fission. EMBO J. *36*, 1330–1347.

Wellen, K.E., Hatzivassiliou, G., Sachdeva, U.M., Bui, T.V., Cross, J.R., and Thompson, C.B. (2009). ATP-citrate lyase links cellular metabolism to histone acetylation. Science *324*, 1076–1080.

Wu, S., and Naar, A.M. (2019). SREBP1-dependent de novo fatty acid synthesis gene expression is elevated in malignant melanoma and represents a cellular survival trait. Sci. Rep. *9*, 10369.

Wu, Y., Chen, K., Liu, X., Huang, L., Zhao, D., Li, L., Gao, M., Pei, D., Wang, C., and Liu, X. (2016). Srebp-1 interacts with c-myc to enhance somatic cell reprogramming. Stem Cells *34*, 83–92.

Wu, Y., Chen, K., Xing, G., Li, L., Ma, B., Hu, Z., Duan, L., and Liu, X. (2019). Phospholipid remodeling is critical for stem cell pluripotency by facilitating mesenchymal-to-epithelial transition. Sci. Adv. *5*, eaax7525.

Yamamoto, T., Hatabayashi, K., Arita, M., Yajima, N., Takenaka, C., Suzuki, T., Takahashi, M., Oshima, Y., Hara, K., Kagawa, K., et al. (2019). Kynurenine signaling through the aryl hydrocarbon receptor maintains the undifferentiated state of human embryonic stem cells. Sci. Signal. *12*, eaaw3306.

Yanes, O., Clark, J., Wong, D.M., Patti, G.J., Sanchez-Ruiz, A., Benton, H.P., Trauger, S.A., Desponts, C., Ding, S., and Siuzdak, G. (2010). Metabolic oxidation regulates embryonic stem cell differentiation. Nat. Chem. Biol. *6*, 411–417.

Yoo, H., Antoniewicz, M.R., Stephanopoulos, G., and Kelleher, J.K. (2008). Quantifying reductive carboxylation flux of glutamine to lipid in a brown adipocyte cell line. J. Biol. Chem. *283*, 20621–20627.

Yoshida, Y., and Yamanaka, S. (2017). Induced pluripotent stem cells 10 years later: for cardiac applications. Circ. Res. *120*, 1958–1968.

Zhang, H., Badur, M.G., Divakaruni, A.S., Parker, S.J., Jager, C., Hiller, K., Murphy, A.N., and Metallo, C.M. (2016). Distinct metabolic states can support self-renewal and lipogenesis in human pluripotent stem cells under different culture conditions. Cell Rep. *16*, 1536–1547.

Zhang, J., Nuebel, E., Daley, G.Q., Koehler, C.M., and Teitell, M.A. (2012). Metabolic regulation in pluripotent stem cells during reprogramming and self-renewal. Cell Stem Cell *11*, 589–595.

**iScience, Volume *23***

## Supplemental Information

# Fatty Acid Synthesis Is Indispensable for Survival of Human Pluripotent Stem Cells

**Sho Tanosaki, Shugo Tohyama, Jun Fujita, Shota Someya, Takako Hishiki, Tomomi Matsuura, Hiroki Nakanishi, Takayo Ohto-Nakanishi, Tomohiko Akiyama, Yuika Morita, Yoshikazu Kishino, Marina Okada, Hidenori Tani, Yusuke Soma, Kazuaki Nakajima, Hideaki Kanazawa, Masahiro Sugimoto, Minoru S.H. Ko, Makoto Suematsu, and Keiichi Fukuda**

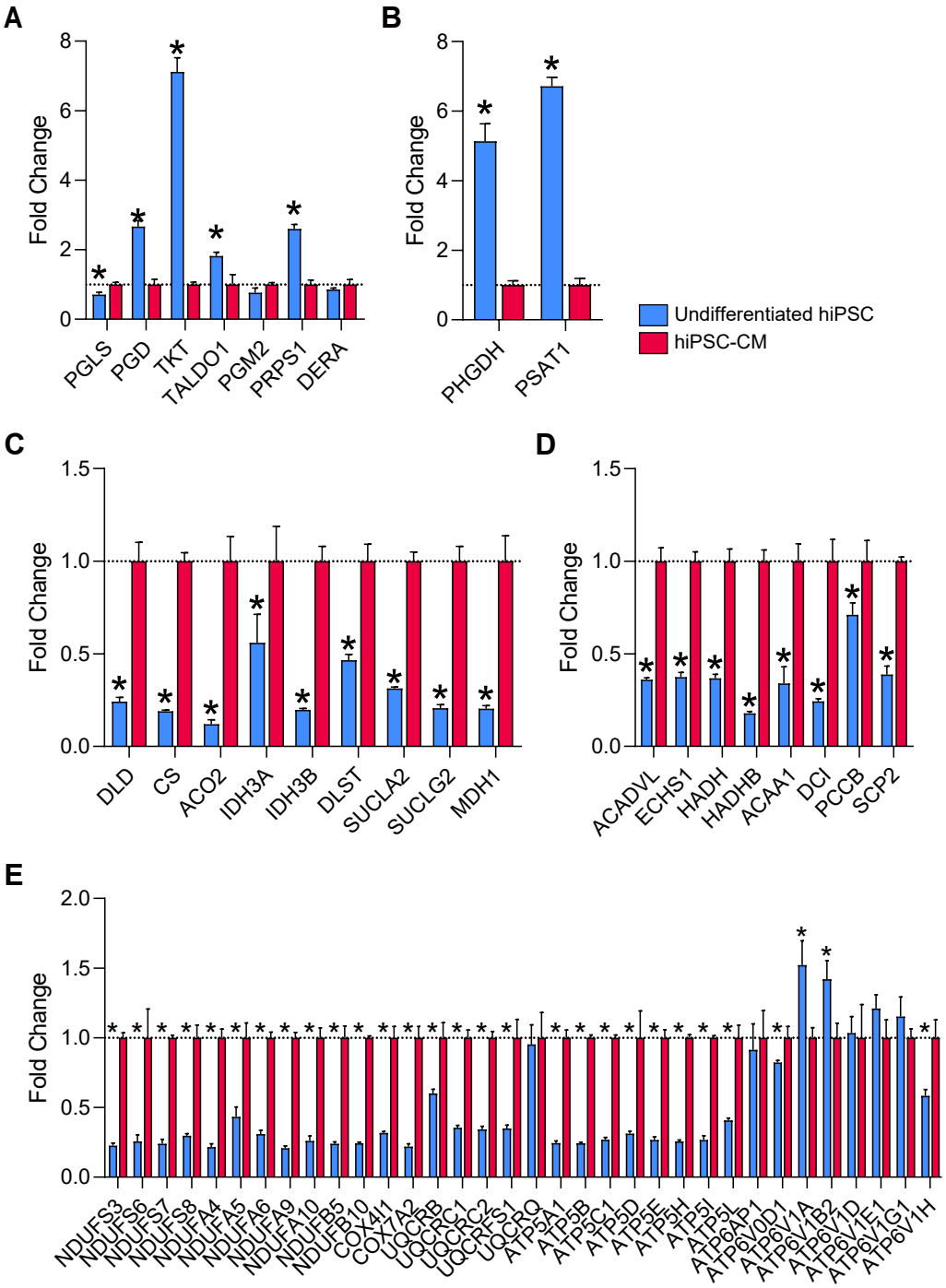
A
B
C
D
E
Fold Change
PGLS
PGD
TKT
TALDO1
PGM2
PRPS1
DERA
PHGDH
PSAT1
Undifferentiated hiPSC
hiPSC-CM
DLD
CS
ACO2
IDH3A
IDH3B
DLST
SUCLA2
SUCLG2
MDH1
ACADVL
ECHS1
HADH
HADHB
ACAA1
DCI
PCCB
SCP2

# Figure S1

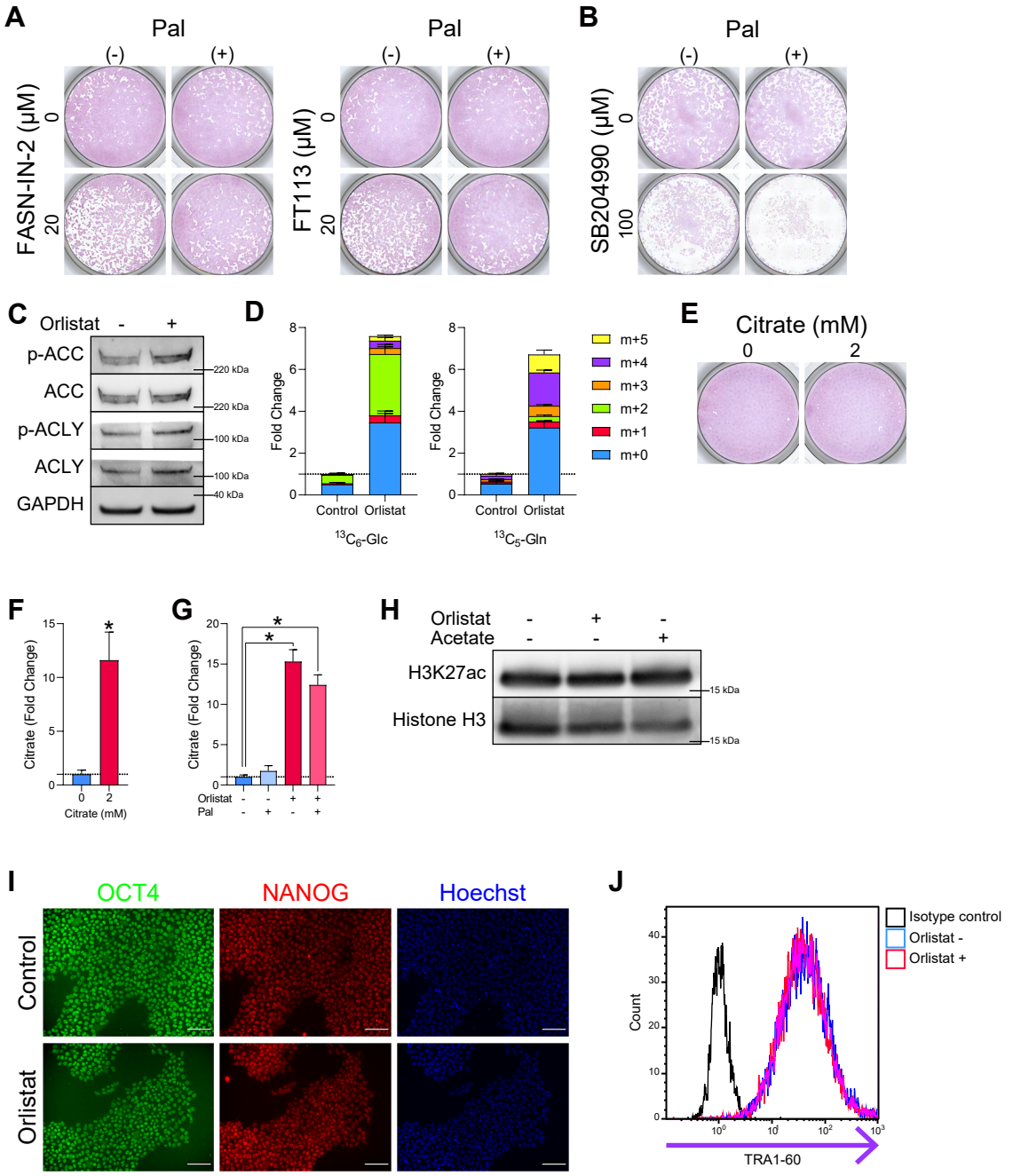
A
Pal
(-)
(+)
FASN-IN-2 (μM)
0
20
FT113 (μM)
B
SB204990 (μM)
100
C
Orlistat
p-ACC
ACC
p-ACLY
ACLY
GAPDH
220 kDa
100 kDa
40 kDa
D
Fold Change
Control
Orlistat
$^{13}C_6$-Glc
$^{13}C_5$-Gln
m+5
m+4
m+3
m+2
m+1
m+0
E
Citrate (mM)
F
Citrate (Fold Change)
G
H
Acetate
H3K27ac
Histone H3
15 kDa
I
OCT4
NANOG
Hoechst
J
Count
TRA1-60
Isotype control
Orlistat -
Orlistat +

Figure S2

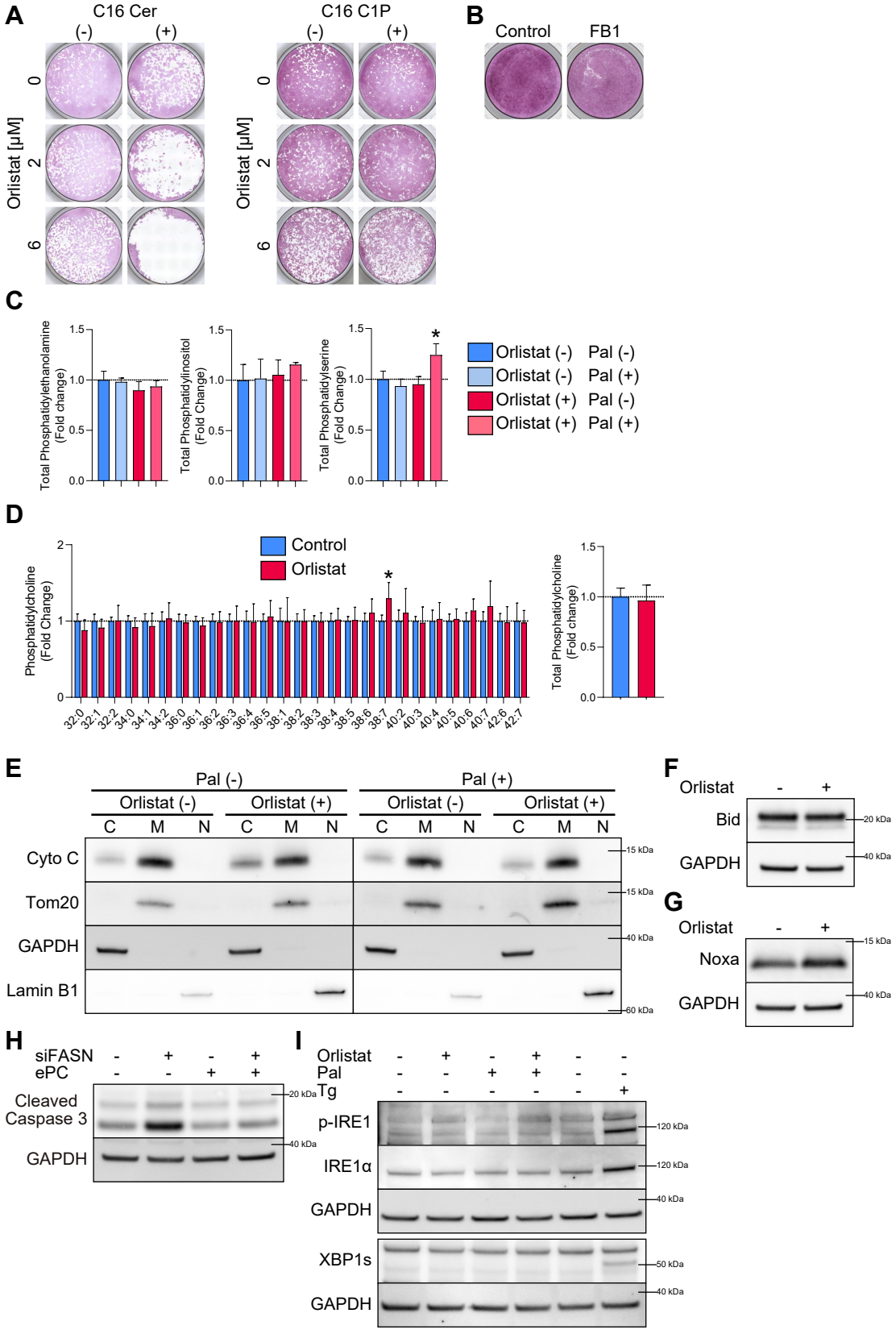
A
C16 Cer
(-)
(+)
C16 C1P
(-)
(+)
Orlistat [μM]
0
2
6
B
Control
FB1
C
Total Phosphatidylethanolamine (Fold change)
Total Phosphatidylinositol (Fold Change)
Total Phosphatidylserine (Fold Change)
Orlistat (-) Pal (-)
Orlistat (-) Pal (+)
Orlistat (+) Pal (-)
Orlistat (+) Pal (+)
D
Control
Orlistat
Phosphatidylcholine (Fold Change)
Total Phosphatidylcholine (Fold change)
32:0
32:1
32:2
34:0
34:1
34:2
36:0
36:1
36:2
36:3
36:4
36:5
38:1
38:2
38:3
38:4
38:5
38:6
38:7
40:2
40:3
40:4
40:5
40:6
40:7
42:6
42:7
E
Pal (-)
Pal (+)
Orlistat (-)
Orlistat (+)
C
M
N
Cyto C
Tom20
GAPDH
Lamin B1
15 kDa
40 kDa
60 kDa
F
Orlistat
Bid
GAPDH
20 kDa
40 kDa
G
Orlistat
Noxa
GAPDH
15 kDa
40 kDa
H
siFASN
ePC
Cleaved Caspase 3
GAPDH
20 kDa
40 kDa
I
Orlistat
Pal
Tg
p-IRE1
IRE1α
GAPDH
XBP1s
GAPDH
120 kDa
120 kDa
40 kDa
50 kDa
40 kDa
J
Control
Orlistat
p53 Hoechst
p53 Hoechst

Figure S3

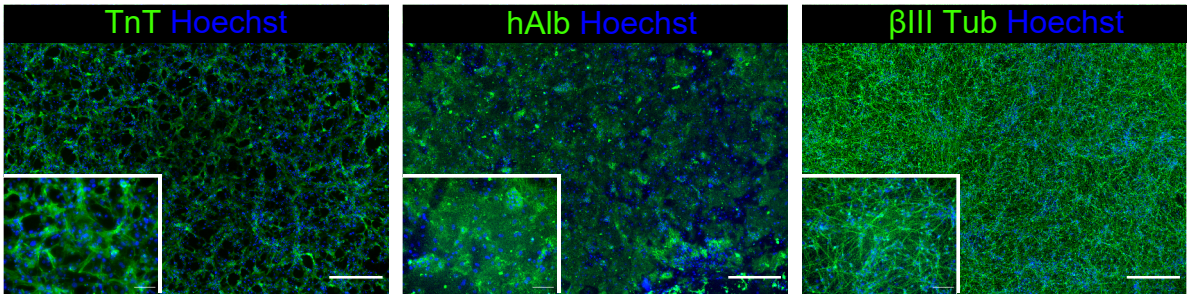


Figure S4

**Supplemental Figure Legends**

**Figure S1 Detailed Proteomics Data, Related to Figure 1**

(A-E) Relative abundance of enzymes related to pentose phosphate pathway (A), serine synthesis pathway (B), TCA cycle (C), FA oxidation (D) and oxidative phosphorylation (E) in hiPSCs (253G4) (blue) and hiPSC (253G4)-CMs (red). Student's *t*-test was performed for each protein (n = 3). Data are presented as means ± S.D. *p < 0.05.

**Figure S2 Palmitic Acid Is Essential for the Survival of Undifferentiated hPSCs, Related to Figure 2**

(A) Representative AP staining image of hiPSCs (253G4) treated with FASN-IN-2 (left) or FT113 (right) and Pal (50 μM) for 24 h.
(B) Representative AP staining image of hiPSCs (253G4) treated with SB204990 and Pal (50 μM) for 24 h.
(C) Representative western blot image showing phosphorylation of ACC (p-ACC) and ACLY (p-ACLY) of hiPSCs (253G4) after 3 h of orlistat treatment.
(D) Stacked bar graphs showing relative change in total amount of citrate, and the percentage of each labeled form (n = 3).
(E) Representative AP staining image of hiPSCs (253G4) treated with 2 mM citrate for 24 h.
(F) CE-MS of citrate in hiPSCs (253G4) after 3 h of 2 mM citrate treatment. Student's *t*-test, n = 3.
(G) CE-MS of citrate in hiPSCs (253G4) after 3 h of 6 μM orlistat and 50 μM Pal treatment. The same concentration of BSA (8.3 μM) was used as a control for Pal. One-way ANOVA with Dunnett's test was performed with orlistat (-) and Pal (-) as a control, n = 3.
(H) Western blotting image of lysine 27 acetylation on histone H3 (H3K27ac) in hiPSCs (253G4) after 12 h of 6 μM orlistat treatment, or 24 h of 10 mM acetate treatment.
(I) Representative image of immunocytochemistry for OCT4 and NANOG in hiPSCs (253G4) after 12 h of 6 μM orlistat treatment. Scale bar: 100 μm.
(J) Flow cytometry analysis of TRA1-60 in hiPSCs (253G4) after 12 h of 6 μM orlistat treatment.

Data are presented as means ± S.D. *p < 0.05.

**Figure S3 Lipidomic Analysis, Exogenous Supplementation of Lipids, and Mechanism of Cell Death, Related to Figure 3**

(A) AP staining of hiPSCs (253G4) treated with orlistat and C16 Cer or C16 C1P for 24 h.

(B) AP staining of hiPSCs (253G4) after 24 h of FB1 treatment.

(C) LC-MS of phosphatidylethanolamine, phosphatidylinositol, and phosphatidylserine of hiPSCs (253G4) after 3 h of 6 μM orlistat treatment, with or without 50 μM Pal. Data are normalized to orlistat (-) Pal (-) as a control. One-way ANOVA with Dunnett's test was performed with orlistat (-) Pal (-) as a control (n = 3).

(D) LC-MS of PC in hiPSC (253G4)-CMs after 3 h of 6 μM orlistat treatment. Data are normalized to controls. Numbers indicate carbon chain lengths followed by degree of desaturation. Student's *t*-test, n = 3.

(E) Representative western blotting image of cytochrome c subcellular localization in hiPSCs (253G4) treated with orlistat and Pal..

(F) Western blotting image of Bid in hiPSCs (253G4) treated with orlistat.

(G) Western blotting image of Noxa in hiPSCs (253G4) treated with orlistat.

(H) Representative western blotting image of cleaved caspase 3 in hiPSCs (253G4) treated with orlistat and chicken egg PC.

(I) Representative western blotting quantification of ER stress response proteins in hiPSCs (253G4) treated with orlistat. The positive control was comprised of 12 h, 3 μM thapsigargin (Tg) treatment. XBP1s, spliced XBP1.

(J) Representative immunocytochemistry images of p53 in undifferentiated hiPSCs (253G4) after 12 h of 6 μM orlistat treatment. Scale bar: 200 μm.

Data are presented as means ± S.D. *$p < 0.05$.

**Figure S4 Immunofluorescent Staining of hiPSC-Derived Cells, Related to Figure 4**

Representative immunocytochemistry images of hiPSC (253G4)-CMs, hepatocytes, and neurons. Scale bar: 500 μm and 100 μm.

## Transparent Methods

### Ethics declarations

The Animal Care and Use Committee of Keio University approved all of the experimental procedures and protocols. This work was conducted in line with the National Institutes of Health Guide for the Care and Use of Laboratory Animals.

### Mouse teratoma model

Male NOG mice (NOD/Shi-scid,IL-2RγKO Jic) aged 6 weeks were purchased from In-Vivo Science. Three days prior to transplantation, $5x10^5$ human dermal fibroblasts(neonatal) (Thermo Fisher Scientific, C0045C) and $0.1x10^5$ undifferentiated hiPSCs (253G4) were plated on 10-cm dishes with StemFit medium, AS103C (Ajinomoto), with or without 6 μM orlistat (Sigma, O4139-25MG). Upon transplantation, cells were rinsed with D-PBS (FUJIFILM Wako Pure Chemical, 045-29795) and incubated with Accutase (Thermo Fisher Scientific, A1110501) for 5 min at 37 °C. Cells were collected with AS103C supplemented with Y-27632 (FUJIFILM Wako Pure Chemical, 034-24024) and centrifuged for 4 min at 300 rcf. Cells were resuspended in diluted Matrigel (Corning, 354230). Supplemented with Y-27632. Orlistat-treated and control cells were transplanted to left and right legs, respectively, of isoflurane-anesthetized mice. Mice were euthanized 8 weeks after transplantation. Tumors were resected and fixed in formaldehyde, followed by hematoxylin-eosin stating. Tumors were observed microscopically by BZ-X710 (Keyence).

### Cell lines

All cells were cultured in a humidified 5% $CO_2$ incubator at 37 °C and routinely tested for mycoplasma contamination.

*hPSCs*

hiPSC lines (253G4, 201B7 and FfI14) were provided by the Center for iPS Cell research and Application, Kyoto University. hESCs line (H9) was provided by WiCELL. The use of hESCs complied with the Guidelines on the Distribution and Utilization of Human Embryonic Stem cells, Ministry of Education, Culture, Sports, Science and Technology, Japan. The hPSCs were maintained with modified StemFit medium, AS103C (Ajinomoto) (Tohyama et al., 2017). Cells were passaged every 4-7 d. Upon passage, cells were washed with D-PBS and incubated for 3 min with TrypLE Select (Thermo Fisher Scientific, 12563-011) at 37 °C. Cells were collected with AS103C supplemented with

10 μM Y-27632 and pelleted for 4 min at 300 rcf. Cells were resuspended and were counted using Vi-CELL (Beckman Coulter). Cells were plated in dishes and plates coated with Matrigel.

*hPSC-derived hepatocytes*

hiPSC-derived hepatocytes (ReproCELL, RCDH001N) were purchased from ReproCELL and cultured according to the manufacturer's instructions. Briefly, 48-well plates were coated with Matrigel. Hepatocytes were thawed at 37 °C and resuspended in ReproHepato Culture Medium (ReproCELL, RCDH101), then pelleted for 5 min at 350 rcf. Cells were resuspended in ReproHepato Culture Medium and replated at 1.8 x $10^5$/well. Medium was changed on days 1, 3, and 5. On day 6, cells were treated with 6 μM orlistat or vehicle control (0.05% dimethyl sulfoxide (DMSO) (Sigma, D250-100ML)) in AS103C.

*hPSC-derived neurons*

hiPSC-derived neurons (ReproCELL, RCDN001N) were purchased from ReproCELL and cultured according to the manufacturer's instructions. Briefly, 48-well plates were coated with poly-L-lysine solution (Sigma, P4832) followed by ReproNeuro Coat (ReproCELL, RCDN201). Neurons were thawed in 37 °C water bath and resuspended in ReproNeuro Culture Medium (ReproCELL, RCDN101), and pelleted for 5 min at 350 rcf. Cells were resuspended in ReproNeuro Culture Medium and replated at 5.6x$10^4$/well. Half of the medium was changed on day 3, 7, and 14. On day 14, cells were treated with 6 μM orlistat or vehicle control (0.05% DMSO) in AS103C medium.

*Human dermal fibroblasts*

Human dermal fibroblasts (neonatal) (Thermo Fisher Scientific, C0045C) were purchased from Thermo Fisher Scientific and were maintained with DMEM (Thermo Fisher Scientific, 11885076) supplemented with 10% FBS (Biowest, S1560-500). Cells were passaged every 4-7 d. Upon passage, cells were washed with D-PBS and incubated for 5 min with trypsin-EDTA solution (NACALAI TESQUE, 35554-64) at 37 °C. Cells were collected with DMEM supplemented with 10% FBS and pelleted for 4 min at 300 rcf. Cells were resuspended and counted using Vi-CELL. Cells were plated in dishes coated with gelatin (Sigma, G9382).

**Cardiomyocyte differentiation from hiPSCs**

The hiPSCs were differentiated to cardiomyocytes as described in previous reports (Burridge et al., 2014; Lian et al., 2013). Briefly, on day 0, cells were rinsed with D-PBS and incubated with RPMI-

1640 (FUJIFILM Wako Pure Chemical, 189-02025) supplemented with 2% B27 supplement without insulin (Thermo Fisher Scientific, A1895601) and 6 μM CHIR99021 (FUJIFILM Wako Pure Chemical, 034-23103) for 1 day. On day 1, cells were rinsed with D-PBS and incubated with RPMI-1640 supplemented with B27 supplement without insulin. On day 3, cells were rinsed with D-PBS and incubated with RPMI-1640 supplemented with B27 supplement without insulin and 5 μM IWR-1 (Sigma, I0161-25MG). On day 6, cells were rinsed with D-PBS and incubated with RPMI-1640 supplemented with B27 supplement without insulin. On day 7, cells were incubated with MEM-α (Thermo Fisher Scientific, 12571-048) supplemented with 5% FBS (Biowest, S1560-500) and 2 mM sodium pyruvate (Sigma, S8636-100ML). On day 12-14, cells were rinsed with D-PBS and incubated for 5 min with trypsin-EDTA solution. Cells were collected with MEM-α supplemented as previously described and were pelleted for 4 min at 300 rcf. Cells were resuspended and counted using Vi-CELL (Beckman Coulter). Cells were plated in dishes coated with collagen type I (AGC TECHNO GLASS, 4020-010). After 2 d, culture medium was replaced to glucose and glutamine-free medium supplemented with 4 mM lactate, StemFit medium AS501 (Ajinomoto) (Tohyama et al., 2016). After 4-7 d, culture medium was replaced by MEM-α, supplemented as previously described. Day 21 or more cardiomyocytes were used for experiments.

**Neural differentiation from hiPSCs using synthetic mRNAs**

hiPSCs (201B7) were differentiated into neurons under feeder-free conditions in StemFit medium, AK02N (Ajinomoto) on laminin-511 (Nippi, 892011)-coated dishes. Neuronal induction was performed by transfection with synthetic mRNA encoding NEUROGENIN2 as previously described (Goparaju et al., 2017). In this experiment, the cells were cultured without a replating step so that undifferentiated cells were remained on the dishes and coexisted with neural cells. The differentiating cells were treated with orlistat for 4 days from day 3 post neuronal induction. For immunostaining, the cells were fixed at day 7.

**Proteomics**

For undifferentiated hiPSCs, cells were rinsed with D-PBS and incubated for 3 min with TrypLE Select in 37 °C. Cells were collected with ice-cold StemFit medium, AS103C, and centrifuged for 4 min at 300 rcf. Supernatant was aspirated and cells were resuspended in ice-cold D-PBS and centrifuged for 4 min at 300 rcf. This procedure was repeated one more time. Following removal of supernatants, cells were resuspended in D-PBS and centrifuged for 5 min at 500 rcf. Supernatant was aspirated and cell pellets were stored at -80 °C and used for proteomic analysis.

For hiPSC-CMs, cell were incubated with prewarmed D-PBS for 3 min at 37 °C. D-PBS was aspirated and cells were incubated with trypsin-EDTA for 5 min at 37 °C. Cells were collected with ice-cold MEMα with 5% FBS and centrifuged for 4 min at 300 rcf. Following procedures were done in the same way as that for undifferentiated hiPSCs and used for proteomic analysis.

Proteomic analysis was performed as previously reported (Matsumoto et al., 2017). Briefly, cell pellets were lysed with 150 µL of 7 M urea (GE Healthcare, 17-1319-01), 2% SDS (Nippon Gene, 311-90271), and 100 mM Tris-HCl, pH 8.8 (Nippon Gene, 311-90391) with sonication by a Bioruptor II (Cosmobio, BR2006A). An equal amount of ultrapure water was added, and sonication was repeated. After centrifugation, the supernatant was used for further analysis. Protein concentrations were measured by a Pierce BCA Protein Assay Kit (Thermo Fisher Scientific, 23225) according to the manufacturer's instructions. Two hundred-µg protein samples were used. Five µL 200 mM Tris-(2-Carboxyethyl)phosphine hydrochloride (Thermo Fisher Scientific, T2556) solution and 5 µL 400 mM 2-iodoacetamide (Sigma, 8.04744) solution were sequentially added to the samples. Proteins were purified by acetone precipitation and precipitates were resuspended in digestion solution (0.5 M triethylammonium bicarbonate buffer (Sigma, T7408-100ML)). Lysyl endopeptidase (FUJIFILM Wako Pure Chemical, 125-05061) solution was added and samples were incubated for 3 h at 37 °C. Four µg trypsin (Thermo Fisher Scientific, 20233) was added and samples were incubated for 3 h at 37 °C. Four µg trypsin was added again and samples were incubated overnight at 37 °C. Protein concentration was measured by Pierce BCA Protein Assay Kit and samples were lyophilized. Proteins were labeled with mTRAQ reagent Δ0 (AB Sciex, 4440015). Samples were lyophilized and stored at -80 °C. Samples were reconstituted with 0.1% trifluoroacetic acid (Merck, 4.80112.2500) to obtain 1 µg/µL solution. Twenty µL of the solution, 4 µL RTM solution (1 µL MRMplus Retention Time Marker (Funakoshi, FMR-002) and 199 µL 0.1% trifluoroacetic acid), 4 µL internal standard peptide solution which contains synthetic peptides (Funakoshi and Genscript) labeled with mTRAQ reagent Δ4 (AB Sciex, 4427698) after reductive alkylation, and 12 µL 0.1% trifluoroacetic acid (Merck, 4.80112.2500) were mixed. The samples were subjected to reversed-phase liquid chromatography (Waters, ACQUITY UPLC H-Class) followed by multiple reaction monitoring analysis (AB Sciex, QTRAP500). The acquired data were analyzed with iMPAQT quant (Kyushu University) and R (R Foundation).

**Immunocytochemistry**

Cells were rinsed with D-PBS and fixed in 4% paraformaldehyde (Muto Pure Chemicals, 33111) for 15-20 min. Cells were treated with 0.1% Triton X-100 (Sigma, T9284) diluted in D-PBS for 5-15 min and rinsed with D-PBS. Cells were treated with blocking solution of either ImmunoBlock (KAC,

CTKN001) or D-PBS with 2% BSA. Cells were treated with primary antibodies diluted in blocking solution at dilutions recommended by manufacturers' instructions at 4 °C overnight. Cells were rinsed with D-BPS twice and were treated with secondary antibodies diluted in blocking solution at dilutions recommended by manufacturer's instructions at room temperature for 2 h. Cells were treated with 5 μg/mL Hoechst 33342 (Thermo Fisher Scientific, H3570) at room temperature for 1 hour or DAPI (Dojindo, D523) at room temperature for 5 min. Cells were imaged using Axio Oberver D1 (Zeiss), BZ-X710 (Keyence), or IX73 (Olympus) microscopes. The mouse monoclonal antibody against OCT4 was purchased from Santa Cruz Biotechnology. The rabbit polyclonal antibody against human NANOG was purchased from ReproCELL. The rabbit polyclonal antibody against FASN was purchased from abcam. The mouse monoclonal antibody against TnT was purchased from Thermo Fisher Scientific. The rabbit monoclonal antibody against p53 and the rabbit monoclonal antibody against βIII Tub were purchased from Cell Signaling. The goat polyclonal antibody against hAlb was purchased from Bethyl Laboratories. The mouse monoclonal antibody against βIII Tub was purchased from Promega. Alexa Fluor 488-labeled anti-mouse IgG, Alexa Fluor 546-labeled anti-mouse IgG, Alexa Fluor 488-labeled anti-rabbit IgG, Alexa Fluor 546-labeled anti-rabbit IgG, and Alexa Fluor 488-labeled anti-goat IgG were purchased from Thermo Fisher Scientific.

**Western blotting**

Cells were treated with indicated reagents or siRNA prior to preparation of samples, then lysed in cell lysate solution (25% NuPAGE™ LDS Sample Buffer (4X) (Thermo Fisher Scientific, NP0007), 10% NuPAGE™ Sample Reducing Agent (10X) (Thermo Fisher Scientific, NP0009), 65% ultrapure water, 1 tablet of PhoSTOP EASYpack (Roche, 4906837001), and 1 tablet of cOmplete™ ULTRA Tablets, Mini, EASYpack Protease Inhibitor Cocktail (Roche, 5892970001)). Lysates were sonicated by an ultrasonic disruptor (TOMY, UR-21P). Protein concentrations were measured by Qubit Protein Assay Kit (Thermo Fisher Scientific, Q33211) and Qubit 3 fluorometer according to the manufacturer's instructions. Electrophoresis and transfer were done according to the manufacturer's instructions. Briefly, proteins were denatured for 10 min at 70 °C. Twenty μg of protein was loaded into each well of a NuPAGE 4-12% Bis-Tris gel (Thermo Fisher Scientific, NP0321BOX). Subsequently, electrophoresis was done by 200V for 35 min in NuPAGE MES SDS running buffer (Thermo Fisher Scientific, NP0002). Transfer was done with iBlot2 PVDF mini Stacks (Thermo Fisher Scientific, IB24002) and an iBlot™ 2 Gel Transfer Device (Thermo Fisher Scientific, IB21001) according to the manufacturer's instructions. Following transfer, membranes were stained with Ponceau-S (Beacle, BCL-PSS-01) for 5 min and rinsed with 1% acetate (FUJIFILM Wako Pure Chemical, 017-00256) for

1-2 min. Membranes were imaged using an iBright FL1000 imaging system (Thermo Fisher Scientific). Membranes were rinsed with TBS-T (TAKAR BIO, T9142) for 3 times 5 min each. Membranes were blocked with Blocking One (NACALAI TESQUE, 03953) for 30 min and rinsed with ultrapure water. Membranes were probed with primary antibodies diluted in TBS-T or TBS-T supplemented with 5% BSA (FUJIFILM Wako Pure Chemical, 019-27051) overnight at 4 °C. Membranes were washed with TBS-T for 3 times 5 min each and probed with secondary antibodies. For chemiluminescence, membranes were probed with horse radish peroxidase-conjugated antibodies at 1:25,000 for 30 min, then washed with TBS-T followed by ultrapure water. Proteins were imaged using ChemiLumi One (NACALAI TESQUE, 07880-70), Pierce™ ECL Plus Western Blotting Substrate (Thermo Fisher Scientific, 32132), or SuperSignal™ West Femto Maximum Sensitivity Substrate (Thermo Fisher Scientific, 34095) with LAS-3000 (FUJIFILM) or iBright FL1000. For fluorescence, membranes were probed with fluorescent secondary antibodies at 1:10,000 for 30 min; membranes were washed three times with TBS-T and imaged with iBright FL1000. The mouse monoclonal antibody against GAPDH was purchased from Thermo Fisher Scientific. The rabbit monoclonal antibodies against p-ACC, ACC, cleaved Caspase 3, and IRE1α and the rabbit polyclonal antibodies against p-ACLY, ACLY, and Bid were purchased from Cell Signaling. The rabbit polyclonal antibodies against H3K27ac, Histone H3, and XBP1; the rabbit monoclonal antibodies against Cyto C and p-IRE1; and the mouse monoclonal antibody against Noxa were purchased from abcam. The mouse monoclonal antibody against Tom20 was purchased from Santa Cruz Biotechnology. The mouse monoclonal antibody against Lamin B1 was purchased from Proteintech. HRP-labeled anti-mouse IgG, HRP-labeled anti-rabbit IgG, and Alexa Fluor 680-labeled anti-mouse IgG were purchased from Thermo Fisher Scientific.

**_FASN_ knockdown in hPSCs**

Undifferentiated hiPSCs were transfected with 10 nM Ambion Silencer Negative Control siRNA (Thermo Fisher Scientific, AM4611) or Ambion *FASN* siRNA (Thermo Fisher Scientific, s5030) using Lipofectamine™ RNAi MAX Transfection Reagent (Thermo Fisher Scientific, 13778030) and Opti-MEM (Thermo Fisher Scientific, 31985070) according to the manufacturer's instructions. The medium was changed 24 h after transfection and cells were incubated for up to 48 h. Proliferation was determined by measuring confluence by IncuCyte ZOOM (Essen Bioscience).

**Alkaline phosphatase staining**

Alkaline phosphatase (AP) staining was performed with Leukocyte AP Kit (Sigma, 86R-1KT) according to the manufacturer's instructions. In brief, cells were rinsed with D-PBS and fixed in 4%

paraformaldehyde at room temperature for 20 min and rinsed with ultrapure water. Cells were then incubated with an alkaline-dye mixture at room temperature overnight. After staining, the dye was removed, and cells were rinsed with ultrapure water.

**Preparation of BSA-conjugated palmitic acid**

BSA-conjugated palmitic acid (Pal) was prepared as described in previous reports (Hannah et al., 2001) with modifications. In brief, Pal (FUJIFILM Wako Pure Chemical, 165-00102) was dissolved in ethanol (FUJIFILM Wako Pure Chemical, 057-00456) and precipitated by adding NaOH (FUJIFILM Wako Pure Chemical, 198-13765). The supernatant was evaporated under stream of nitrogen. The precipitate was reconstituted with 0.9%w/v NaCl (FUJIFILM Wako Pure Chemical, 191-01665) and 10%w/v fatty acid-free BSA (FUJIFILM Wako Pure Chemical, 017-15146) at a molecular ratio of 6:1. The solution was adjusted to pH 7.0 with HCl (FUJIFILM Wako Pure Chemical, 080-01066).

**LIVE/DEAD assay**

The LIVE/DEAD assay (Thermo Fisher Scientific, L3224) )was performed according to the manufacturer's instructions. In brief, half of the culture medium was aspirated, calcein AM and ethidium homodimer-1 dissolved in D-PBS were added to the medium, and cells were incubated at 37 °C for 30 min. Medium and D-PBS were changed to culture medium and cells were examined using a microscope.

**Capillary electrophoresis-mass spectrometry**

Capillary electrophoresis time-of-flight mass spectrometry (CE-TOFMS) was performed as previously described (Ohmura et al., 2015; Shiota et al., 2018; Yamamoto et al., 2014). Briefly, cells were rinsed with D-PBS and cultured under the conditions described above for 3 h. Cells were rinsed with ice-cold 5 % (w/v) mannitol (FUJIFILM Wako Pure Chemical, 137-00843) twice and collected with methanol (FUJIFILM Wako Pure Chemical, 138-06473) that contained 300 mM methionine sulfone and 300 mM 2-morpholinoethanesulfonic acid as internal and external standards, respectively. The protocols of hydrophilic metabolites extraction, as well as the instrument specifications, and measurement conditions were described previously (Koh et al., 2013). Briefly, metabolites were extracted from cells with a extraction solvent [methanol:water:chloroform = 1:0.5:1 (v/v/v)]. The extract was centrifuged at 20,000 *x g* and 4 °C for 15 minutes. The water and methanol layer was filtered using a 5 kDa cut-off filter (UFC3LCCNB, Human Metabolome Technologies, Tsuruoka, Japan). The filtrate was lyophilized and dissolved in deionized water containing 3-aminopyrrolidine

and trimesate (200 mM each) as reference compounds. Metabolites were analyzed using an Agilent CE-TOFMS system equipped with an Agilent G7100A CE instrument, and an Agilent 6530 Q-TOF LC/MS system (Agilent Technologies). Raw data were processed using MasterHands (Sugimoto et al., 2010). The metabolites were identified by matching m/z and corrected migration times with those in our standard library. The absolute concentration was quantified based on the ratio among peak areas of each metabolite, internal, and external standard compounds.

**Liquid chromatography-mass spectrometry**

Cells were rinsed with D-PBS and then collected with 0.25 mM trypsin-EDTA followed by pelleting at 300 g for 4 min. Cell pellets were stored for further analysis.

*Lipid preparation*

A comprehensive lipid analysis was done as described previously (Shindou et al., 2017; Yamamoto et al., 2018). Briefly, total lipids were extracted using the Bligh-Dyer method (Bligh and Dyer, 1959). Anionic phospholipids (PLs) including phosphatidic acid, phosphatidylserine, phosphatidylinositol, phosphatidylglycerol, lysophosphatidic acid, lysophosphatidylserine, lysophosphatidylinositol, lysophosphatidylglycerol, C1P, sphinganine-1-phosphate, and sphingosine-1-phosphate were condensed using a diethylaminoethyl-cellulose column (Santa Cruz Biotechnology) and subjected to methylation by trimethylsilyldiazomethane (Kielkowska et al., 2014). Samples of the organic layer were dried under a gentle stream of nitrogen and then dissolved in methanol for LC/MS/MS measurements.

*MS analyses of phospholipids*

The samples were analyzed using an electrospray ionization- triple-stage quadrupole mass spectrometer (TSQ Vantage AM, Thermo Fisher Scientific) interfaced with an UltiMate 3000 LC system (Thermo Fisher Scientific). The samples were subjected to LC-ESI-MS/MS analysis using the Waters X-Bridge C18 columns (3.5 μm, 150 mm × 1.0 mm i.d.). Samples were simply injected via the HTC PAL autosampler (CTC Analytics), and the PL fractions were separated by a linear gradient composed of different ratios of mobile phase A [isopropanol/methanol/water (5/1/4 v/v/v) supplemented with 5 mM ammonium formate and 0.05% ammonium hydroxide (28% in water)] and mobile phase B [isopropanol supplemented with 5 mM ammonium formate and 0.05% ammonium hydroxide (28% in water)]. The linear gradient increased from 40% to 60% B in 1 min, from 60% to 80% B for the next 8 minutes, from 80% to 95% B during the next 2 min, and was then kept at 95%

B for 19 min with a flow rate of 25 μL/min and a column temperature of 25 ℃. Lipid species were measured using selected reaction monitoring (SRM) in the positive ion mode. Characteristic fragments of individual lipids were detected via the product ion scan (MS/MS mode).

*MS analyses of triacylglycerol*

Analyses were performed on an LC/MS/MS system consisting of a Q-Exactive Plus mass spectrometer (Thermo Fisher Scientific, Waltham, MA, USA) equipped with an electrospray ionization (ESI) source and an UltiMate 3000 system (Thermo Fisher Scientific). Lipid samples were separated using a Waters X-Bridge C18 column (3.5 μm, 150 mm × 1.0 mm i.d.) at 40°C, and a linear gradient composed of different ratios of mobile phase A [isopropanol/methanol/water (5/1/4 v/v/v) supplemented with 5 mM ammonium formate and 0.05% ammonium hydroxide (28% in water)], and mobile phase B [isopropanol supplemented with 5 mM ammonium formate and 0.05% ammonium hydroxide (28% in water)]: ratios of 60/40% (0 min), 40/60% (1 min), 20/80% (9 min), 5/95% (11-30 min), 95/5% (31-35 min) and 60/40% (35-45 min). The flow rate was 25 μL/min. The source and ion transfer parameters applied were as follows: spray voltage 4.0 kV. For positive ionization modes, the sheath gas and the capillary temperature were maintained at 10 and 320 °C, respectively. The Orbitrap mass analyzer was operated at a resolving power of 70,000 in full-scan mode (scan range 600–2000 m/z; automatic gain control (AGC) target 1e6) and of 17,500 in the Top 20 data-dependent MS2 mode (stepped normalized collision energy 20, 30 and 40; isolation window 4.0 m/z; AGC target 1e5) with a dynamic exclusion setting of 10.0 s. Identification of TAG molecular species was performed using the LipidSearch4.2 software (Mitsui knowledge industry CO., LTD.).

**Liposome preparation**

Liposomes were prepared as previously described (Mendez and Banerjee, 2017; Szoka and Papahadjopoulos, 1980). Briefly, lipids dissolved in chloroform (FUJIFILM Wako Pure Chemical, 038-02606) were dried in a stream of nitrogen gas to form a lipid film. The film was reconstituted in medium and sonicated with an ultrasonic bath (Branson, CPX2800H-J) to produce liposomes. One percent penicillin-streptomycin (Thermo Fisher Scientific, 15140122) was supplemented to the medium.

**Flow cytometry**

Cells were rinsed with D-PBS and incubated for 3 min with TrypLE Select at 37 °C. Cells were collected with AS103C and counted using Vi-CELL. They were then pelleted for 3 min at 300 rcf and resuspended in D-PBS supplemented with 2% FBS. A total of 1 x $10^6$ cells were aliquoted and

supplemented with 10 µL of primary antibodies conjugated with phycoerythrin for 30 min on ice. Cells were rinsed with D-PBS and pelleted for 3 min at 300 rcf. They were then resuspended in D-PBS supplemented with 2% FBS and analyzed with Gallios 2L6C (Beckman Coulter). PE-labeled Isotype control antibody and PE-labeled antibody against TRA1-60 were purchased from Miltenyi Biotec.

**Quantification and statistical analysis**

All statistical analyses were carried out using SPSS (IBM) or GraphPad Prism (GraphPad). Values are presented as means ± S.D. Statistical significance was evaluated using the Student's *t*-test for comparisons between two groups and one-way ANOVA followed by Dunnett's multiple comparison test for multiple comparisons between more than two groups unless otherwise specified. A value of $p < 0.05$ was considered significant.

**Supplemental References**


Bligh, E.G., and Dyer, W.J. (1959). A rapid method of total lipid extraction and purification. Can. J. Biochem. Physiol. *37*, 911–917.

Burridge, P.W., Matsa, E., Shukla, P., Lin, Z.C., Churko, J.M., Ebert, A.D., Lan, F., Diecke, S., Huber, B., Mordwinkin, N.M., et al. (2014). Chemically defined generation of human cardiomyocytes. Nat. Methods *11*, 855–860.

Goparaju, S.K., Kohda, K., Ibata, K., Soma, A., Nakatake, Y., Akiyama, T., Wakabayashi, S., Matsushita, M., Sakota, M., Kimura, H., et al. (2017). Rapid differentiation of human pluripotent stem cells into functional neurons by mRNAs encoding transcription factors. Sci. Rep. *7*, 42367.

Hannah, V.C., Ou, J., Luong, A., Goldstein, J.L., and Brown, M.S. (2001). Unsaturated fatty acids down-regulate srebp isoforms 1a and 1c by two mechanisms in HEK-293 cells. J. Biol. Chem. *276*, 4365–4372.

Kielkowska, A., Niewczas, I., Anderson, K.E., Durrant, T.N., Clark, J., Stephens, L.R., and Hawkins, P.T. (2014). A new approach to measuring phosphoinositides in cells by mass spectrometry. Adv. Biol. Regul. *54*, 131–141.

Koh, T., Murakami, Y., Tanaka, S., Machino, M., Onuma, H., Kaneko, M., Sugimoto, M., Soga, T., Tomita, M., and Sakagami, H. (2013). Changes of metabolic profiles in an oral squamous cell carcinoma cell line induced by eugenol. In Vivo *27*, 233-243.

Lian, X., Zhang, J., Azarin, S.M., Zhu, K., Hazeltine, L.B., Bao, X., Hsiao, C., Kamp, T.J., and Palecek, S.P. (2013). Directed cardiomyocyte differentiation from human pluripotent stem cells by modulating Wnt/beta-catenin signaling under fully defined conditions. Nat. Protoc. *8*, 162–175.

Matsumoto, M., Matsuzaki, F., Oshikawa, K., Goshima, N., Mori, M., Kawamura, Y., Ogawa, K., Fukuda, E., Nakatsumi, H., Natsume, T., et al. (2017). A large-scale targeted proteomics assay resource based on an in vitro human proteome. Nat. Methods *14*, 251–258.

Mendez, R., and Banerjee, S. (2017). Sonication-based basic protocol for liposome synthesis. Methods Mol. Biol. *1609*, 255–260.

Ohmura, M., Hishiki, T., Yamamoto, T., Nakanishi, T., Kubo, A., Tsuchihashi, K., Tamada, M., Toue, S., Kabe, Y., Saya, H., et al. (2015). Impacts of CD44 knockdown in cancer cells on tumor and host metabolic systems revealed by quantitative imaging mass spectrometry. Nitric Oxide *46*, 102–113.

Shindou, H., Koso, H., Sasaki, J., Nakanishi, H., Sagara, H., Nakagawa, K.M., Takahashi, Y., Hishikawa, D., Iizuka-Hishikawa, Y., Tokumasu, F., et al. (2017). Docosahexaenoic acid preserves visual function by maintaining correct disc morphology in retinal photoreceptor cells. J. Biol. Chem. *292*, 12054–12064.

Shiota, M., Naya, M., Yamamoto, T., Hishiki, T., Tani, T., Takahashi, H., Kubo, A., Koike, D., Itoh, M., Ohmura, M., et al. (2018). Gold-nanofeve surface-enhanced Raman spectroscopy visualizes hypotaurine as a robust anti-oxidant consumed in cancer survival. Nat. Commun. *9*, 1561.

Sugimoto, M., Wong, D.T., Hirayama, A., Soga, T., and Tomita, M. (2010). Capillary electrophoresis mass spectrometry-based saliva metabolomics identified oral, breast and pancreatic cancer-specific profiles. Metabolomics *6*, 78–95.

Szoka, F., Jr., and Papahadjopoulos, D. (1980). Comparative properties and methods of preparation of lipid vesicles (liposomes). Annu. Rev. Biophys. Bioeng. *9*, 467–508.

Tohyama, S., Fujita, J., Fujita, C., Yamaguchi, M., Kanaami, S., Ohno, R., Sakamoto, K., Kodama, M., Kurokawa, J., Kanazawa, H., et al. (2017). Efficient large-scale 2D culture system for human induced pluripotent stem cells and differentiated cardiomyocytes. Stem Cell Rep. *9*, 1406–1414.

Yamamoto, T., Endo, J., Kataoka, M., Matsuhashi, T., Katsumata, Y., Shirakawa, K., Yoshida, N., Isobe, S., Moriyama, H., Goto, S., et al. (2018). Decrease in membrane phospholipids unsaturation correlates with myocardial diastolic dysfunction. PLoS One 13, e0208396. doi: 10.1371/journal.pone.0208396.

Yamamoto, T., Takano, N., Ishiwata, K., Ohmura, M., Nagahata, Y., Matsuura, T., Kamata, A., Sakamoto, K., Nakanishi, T., Kubo, A., et al. (2014). Reduced methylation of PFKFB3 in cancer cells shunts glucose towards the pentose phosphate pathway. Nat. Commun. *5*, 3480.